Analyst

ROYAL SOCIETY OF CHEMISTRY

CRITICAL REVIEW

View Article Online
View Journal | View Issue

Cite this: *Analyst*, 2025, **150**, 3045

Recent progress of dual-responsive fluorescent probes for polarity and analytes

Junru He,[a] Xuwei Han[b] and Yongkang Yue *[b]

Polarity, as an indicator of the cellular microenvironment, regulates cell functions in conjunction with bioactive molecules including proteins, ROS, RNS, RSS, *etc*. Their synergistic effect is closely linked to the emergence and advancement of atherosclerosis, diabetes, cancer and neurodegenerative diseases. Accordingly, monitoring the collaborative changes to polarity and related biomolecules in real time is important and illustrates their biological and pathological roles. Fluorescence imaging revealed substantial benefits and prospects for the identification of the micro-environment and analytes in organisms due to its high resolution, non-invasiveness, and real-time monitoring features. In this review, we summarized progress made in research on multifunctional fluorescent probes for the simultaneous tracking of polarity and analytes in the past five years. Our focus centered on the design approaches, spectral properties and biological utilization of current multifunctional fluorescent probes for detecting polarity and analytes, and we analyzed their limitations and prospects. We anticipate that this review will inspire a panoramic understanding of the relationship between polarity and various biologically active molecules, and promote the further design of new probes for a deeper illustration of invisible biomechanisms.

Received 4th March 2025,
Accepted 31st May 2025

DOI: 10.1039/d5an00243e

rsc.li/analyst

Introduction

Polarity is an essential microenvironment-related parameter, and it has been proved to be involved in numerous physiological processes, including enzyme conformation regulation, membrane fusion, the sensitization of proteins and the composition of lipids.[1–5] Anomalous polarity variations were linked to cellular malfunction and the occurrence of many diseases.[6–11] Firstly, many studies have shown that cancer cells have a higher metabolism for lipid synthesis and more diverse lipid signaling, resulting in cancer cells displaying lower polarity than normal cells.[12–16] Secondly, in protein conformation diseases such as neurodegenerative diseases, protein misfolding or precipitation due to abnormal aggregation can occur under aging or other harmful stresses, resulting in polarity changes during this process.[17,18] Likewise, interactions between proteins are also capable of influencing the polarity of the interfacial region as well.[19–21] In addition, the asymmetric distribution of membrane lipids is disrupted, and stressors such as oxidation can lead to polarity changes among organelles.[22–24] Overall, the development of chemical probes to address these polarity issues has pathological and physiological significance for disease diagnosis and research into mechanisms.[25–28]

Polarity and most small biomolecules in living organisms cannot be analyzed *in vitro*; it can only be achieved by exploiting the *in situ* analysis capability of fluorescent probes.[29–31] In recent years, with the rapid development of fluorescence imaging technology, small molecule fluorescent probes have been widely applied owing to their potential advantages such as simple operation, high sensitivity, non-invasive detection, real-time monitoring, and low cost.[32–39] Furthermore, by using advanced instruments and techniques such as fluorescence confocal microscopy (FCM), fluorescence lifetime imaging microscopy (FLIM), and two-photon imaging microscopy (TPE), fluorescent probes could be better used for performing non-invasive determination of pertinent analytes, providing technical support for further pathological and physiological research.[40–42] In vital processes, multiple parameters may fluctuate simultaneously.[43] For example, variations in cell polarity and analyte contents can emerge concurrently.[43–45] In this case, although the concurrent application of two selective probes for the detection of dual indicators remains conceptually feasible, even the slightest disparities in the take up, localization, and retention of the two probes will undermine the interpretation of data.[46] This fundamental limitation underscores the critical advantages (such as enhancing the sensitivity and specificity of imaging, more accurate diagnosis of related diseases) of integrating dual sensing modalities

[a]*School of Chemistry and Chemical Engineering, Shanxi University, Taiyuan 030006, China*
[b]*Key Laboratory of Chemical Biology and Molecular Engineering of Ministry of Education, Key Laboratory of Materials for Energy Conversion and Storage of Shanxi Province, Institute of Molecular Science, Shanxi University, Taiyuan 030006, China. E-mail: ykyue@sxu.edu.cn*

within a single molecular architecture.[47] Therefore, it is extremely necessary to develop multi-functional fluorescent probes.[48,49]

The recognition and sensing mechanisms of most existing multi-functional fluorescent probes mainly involve ICT (intramolecular charge transfer),[50,51] TICT (twisted intramolecular charge transfer),[52] PET (photoinduced electron transfer),[53,54] and ESIPT (excited-state intramolecular proton transfer).[55,56] The correct understanding of these fluorescence mechanisms will be a prerequisite for the construction and utilization of versatile fluorescent probes. Probes based on the ICT mechanism typically comprise a π-conjugated system connecting an electron donor (D) and electron acceptor (A), with a typical D–π–A structure. When this type of probe interacts with the analyte, the density of electrons in the molecule changes, resulting in variations in the interactions between the molecule and solvent dipole, which are presented by changes to the fluorescence emission intensity and wavelength. TICT represents a common photophysical occurrence in the D–π–A system, where the electron-donating and electron-accepting parts of these molecules are usually connected by a rotating bond. When the rotation of the rotor within the molecule is inhibited by environmental factors, TICT is obstructed and the probe exhibits enhanced fluorescence. Probes based on the PET mechanism also have three parts: electron donor, acceptor, and linker. PET probes can be categorized into two types: (1) excited fluorophores act as A, and electrons shift from the donor component to the fluorophores, that is, an acceptor-excited PET (a-PET); and (2) electrons undergo transfer from the excited fluorophore as a donor to the electron acceptor, *i.e.* donor-excited PET (d-PET). PET probes themselves exhibit quenching of the excited state fluorescence. However, when the recognition group binds to the analyte, the PET process is inhibited and the fluorescence of the probe is enhanced. This type of probe is usually "off–on" with low biological background and high sensitivity. ESIPT refers to the process in which protons within the molecule are excited, and then transferred to adjacent atoms through intramolecular hydrogen bonds, resulting in the formation of tautomers. ESIPT molecules undergo instantaneous electron arrangement and relaxation, resulting in a large Stokes shift between the absorption spectrum and fluorescence emission spectrum, which can effectively eliminate fluorescence quenching caused by self-absorption and greatly improve detection accuracy.

To date, a series of reviews have reported on single fluorescent probes applied for the detection of polarity or analytes.[57–65] Nevertheless, few reviews concentrated on the progress made in creating versatile fluorescent probes for the concurrent identification of polarity and other analytes. In view of this observation, we firstly summarize progress made in the last 5 years for fluorescent probes used to concurrently detect polarity and analytes. The design approaches for versatile fluorescent probes with respect to polarity and analytes can be mainly classified into three categories (Fig. 1): (1) a probe with a long D–π–A conjugation system emits bright fluorescence in the long wavelength channel, the fluorescence emission is red-shifted with increasing polarity, and when it combines with analytes, their conjugation structure is disrupted/altered, exhibiting enhanced fluorescence in the short wavelength channel. (2) Probes react with analytes, the generated product shows significantly enhanced fluorescence only in the low polarity environment, and through this sequential cascade reaction, the detection of the analyte is achieved. (3) The probe responds to polarity and the analyte through different mechanisms in different emission channels; during the response process, neither environmental polarity nor interactions with other analytes compromise the structural integrity of the probe molecule. Herein, the review focuses on three aspects, namely, the design concept, spectral properties, and biological application of multifunctional fluorescent probes, and further summarizes and gives an outlook on them (Scheme 1). We anticipate that it will contribute to research on linkages and crosstalk between polarity and analytes in interrelated pathophysiological processes.

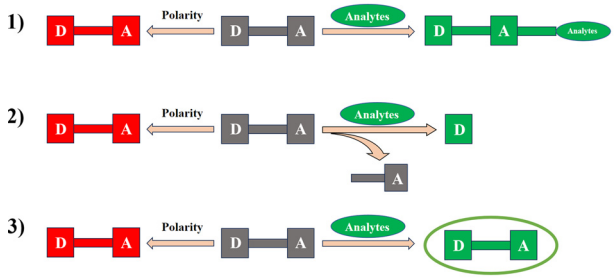

Fig. 1 Design approaches for multifunctional fluorescent detectors with respect to polarity and analytes.

Polarity and analyte detection with versatile fluorescent probes

Polarity and ROS

Singlet oxygen ($^1O_2$), hydroxyl radicals ($^{\bullet}OH$), superoxide radicals ($O_2^{\bullet-}$), hydrogen peroxide (H_2O_2), and hypochlorous acid (HClO) are the main components of reactive oxygen species (ROS).[66,67] ROS, as a messenger molecule, is crucial for maintaining the redox balance during physiological processes.[68] In some physiological and pathological processes, such as oxi-

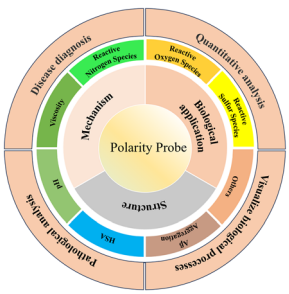

Scheme 1 Overview of fluorescent probes for detecting polarity and analytes.

dative stress and inflammation, in which ROS and polarity are involved concurrently, their abnormal levels will lead to neurodegenerative diseases, cancer, kidney disease, diabetes and other diseases.[69] Therefore, it is necessary to develop an effective platform to simultaneously monitor the fluctuations in polarity and ROS in the biological environment.

In 2021, Yan *et al.*[70] reported the dual functional fluorescent probe CTPA, with ICT and AIE characteristics, for the determination of HClO and polarity at different emission channels. As depicted in Fig. 2(a), in the molecular structure of the CTPA probe, 7-hydroxycoumarin was selected as the fluorophore, and *N*,*N*-dimethylthiocarbamate was used as the recognition group for ClO^-. Meanwhile, the introduction of the triphenylamine (TPA) group made the probe sensitive to polarity. Specifically, when ClO^- was introduced, the CTPA probe exhibited significant fluorescence enhancement at 456 nm and reached a plateau within 30 s, showing high selectivity and sensitivity (LOD = 11.9 nM). In addition, there

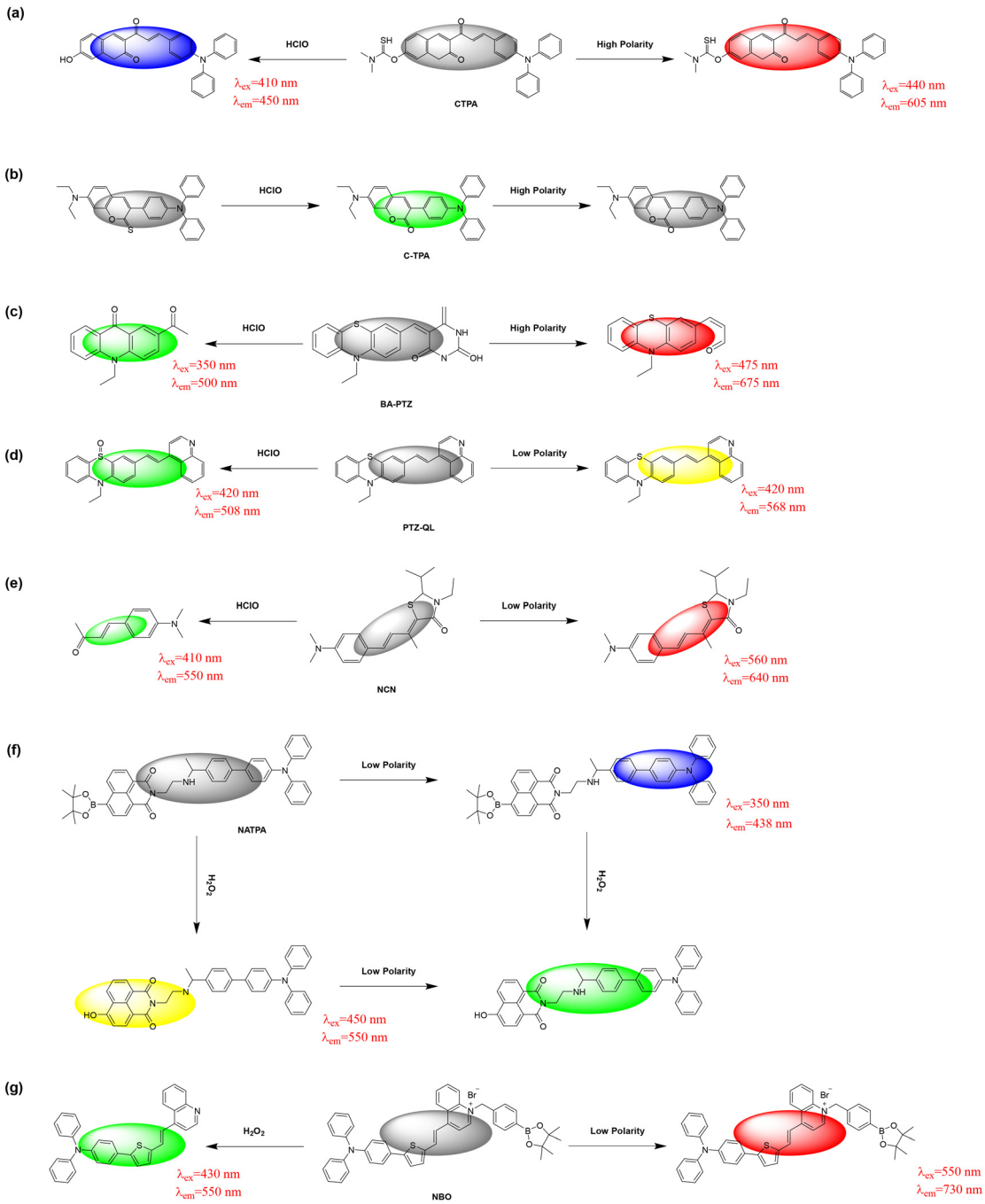

Fig. 2 Fluorescent probes for detecting polarity and ROS.

was a reduction in the fluorescence intensity as the level of polarity rose, and the maximum emission of the CTPA probe presented a redshift from 549 to 604 nm, realizing a response to polarity variation. In addition, given the minimal toxicity and excellent membrane passing ability of CTPA, it was successfully used for the imaging of ClO^- and polarity in HeLa cells and HIN-3T3 cells, and identified these two types of cells *via* ClO^- and polarity. Therefore, the CTPA probe will be a promising tool for studying the relationship between ClO^- and polarity in the complex physiological system.

In 2022, another probe, C–TPA (Fig. 2(b)), capable of detecting ClO^- and polarity was constructed by Zuo's group.[71] This probe had a similar molecular framework to that of CTPA, featuring coumarin and triphenylamine (TPA) as core structural components. In contrast to CTPA, C–TPA innovatively used the classic sulfurization reagent, Laveson reagent, which converted carbonyl groups into thiocarbonyl groups, to mediate a dynamic ClO sulfurization strategy. Regarding the detection performance, compared to CTPA with stronger electron withdrawing thiocarbamate groups, the sensitivity of C–TPA was inferior to that of CTPA, with a LOD of 0.12 μM. However, C–TPA demonstrated diagnostic advantages by distinguishing tumor tissues *via* LDs polarity gradients. Notably, neither probe addressed reversibility – a critical gap for monitoring transient oxidative bursts. Future designs could hybridize the AIE scaffold of CTPA with the thiation chemistry of C–TPA to engineer stimuli-responsive probes for real-time redox dynamics monitoring.

Ferroptosis (FPT) is a regulated cell self-destruction pathway dependent on iron, and it has received widespread attention due to its association with diverse illnesses such as cancer, Parkinson's disease, Alzheimer's disease (AD), and cardiovascular disease.[72–74] ROS and lipid peroxidation levels are key markers of FPT.[75] In 2023, Xu and his colleagues[76] came up with an innovative NIR fluorescent probe, BA–PTZ (Fig. 2(c)), which contained barbituric acid as the hydrophilic moiety and phenothiazine acted as the lipophilic component. The biphasic framework of BA–PTZ enabled it to specifically target LDs. Also, phenothiazine was specifically subjected to oxidation by HClO, resulting in it being changed into a sulfoxide. When HClO was present, it could induce fluorescence enhancement of BA–PTZ by about 100 times within 20 s, with a LOD as low as 37 nM. In addition, co-localization imaging experiments showed that BA–PTZ had excellent LD staining specificity (Pearson correlation coefficient (PCC = 0.90)), and it was capable of responding to changes in cell polarity in the NIR emission region. In the case where HeLa cells were exposed to HClO and oleic acid, respectively, the polarity change of LDs and HClO in HeLa cells could be easily detected. In addition, by introducing a cell model of FPT, the probe successfully detected changes in HClO and polarity during FPT, which was beneficial for determining the occurrence of FPT and related biological processes.

Recently, He *et al.*[77] also developed a series of dual ratio fluorescent probes using the phenothiazine group to simultaneously monitor the dynamic changes in ClO^- and polarity during FPT. These probes all had a donor–acceptor (D–A) structure in which the phenothiazine moiety was used as an electron-donating substance and reactive site toward ClO^- oxidation. Among them, the PTZ–QL probe (Fig. 2(d)) with NIR fluorescence emission displayed a unique fluorescence response to ClO^- and polarity change: when ClO^- was added, the fluorescence shifted from 712 nm to 508 nm. As the polarity decreased, the fluorescence changed from 661 nm in DMSO to 554 nm in 1,4-dioxane. The probe could image the response to ClO^- and polarity in living cells using laser confocal imaging. Furthermore, using erastin to induce FPT, the probe was cleverly utilized to observe the increase in ClO^- concentration and polarity in ratio imaging during the FPT process.

Based on the above discussion, we could summarize that these two phenothiazine (PTZ)-based probes detected microenvironmental changes through polarity-responsive mechanisms (ICT/TICT) and monitored ClO^-/HClO *via* oxidation reactions. The difference lay in PTZ–QL exhibiting dual-ratiometric signals, while BA–PTZ showed only NIR enhancement. Additionally, BA–PTZ had the advantage of LD targeting, providing a novel tool for *in vivo* microenvironment monitoring. In terms of applications, both probes focused on ferroptosis research. Moving forward, researchers can develop next-generation probes with high sensitivity, precise targeting, and *in vivo* compatibility through structural optimization and multi-modal integration, thereby advancing research on the ferroptosis mechanism and its clinical translation.

A NIR fluorescent probe, NCN (Fig. 2(e)), with dimethylaniline as the fluorophore was designed based on the π-bridge connection strategy by Yang *et al.*[78] The probe could target LDs and simultaneously monitor HClO and viscosity/polarity variation in live cells. When the viscosity increased or the polarity decreased, NCN exhibited a sharp fluorescence enhancement in the region of 640–670 nm. Meanwhile, as the amount of HClO increased, the fluorescence emitted at 550 nm became significantly enhanced by 151 times and reached a plateau within 12 min (LOD = 11.84 nM). In cell imaging, the upregulation of HClO and the increase in viscosity (decrease in polarity) were detected through dual channel emission during FPT. Additionally, the use of NCN dual channel imaging successfully achieved the visualization of inflammation, non-alcoholic fatty liver disease (NAFLD), and cancerous tissues/organs in living mice. These findings revealed that NCN was an effective tool for the early diagnosis of the above-mentioned related diseases.

Yan's group developed the dual site fluorescent probe NATPA for concurrent imaging of intracellular H_2O_2 and polarity.[79] As shown in Fig. 2(f), NATPA utilized ethylenediamine to connect naphthalimide and TPA to avoid crosstalk between them. The borate group attached to naphthalimide served as the recognition site for H_2O_2, and its response to polarity was based on the ICT effect existing in the typical D–π–A skeleton of NATPA. NATPA exhibited excellent spectral performance in response to H_2O_2, including high sensitivity (LOD = 44 nM), selectivity, and a rapid response (15 min).

Simultaneously, it showed sensitive response behavior to polarity, independent of pH and viscosity. In addition, the probe could target LDs, and successfully distinguished between the HepG2 and LO2 cells based on the higher concentration of H_2O_2 and lower polarity in cancer cells. NATPA also provides an idea for the construction of dual site fluorescent probes for the simultaneous detection of active molecules and polarity. Recently, Tian *et al.*[80] constructed a highly sensitive dual channel TPA-based fluorescent probe, NBO (Fig. 2(g)), with an AIE effect for the detection of H_2O_2 and polarity. Compared to NATPA, this probe extended the fluorescence emission to the NIR region, which was beneficial for deeper tissue imaging and low biological background interference. NBO had the characteristics of a large Stokes shift (180 nm), good photostability, and low cytotoxicity. In addition, NBO successfully achieved the recognition of cancer cells by imaging intracellular H_2O_2 and polarity. Importantly, imaging experiments on cells and mice indicated that NBO could visualize abnormalities in H_2O_2 and polarity in inflammation and FPT models.

Polarity and RSS

Reactive sulfur species (RSS), including hydrogen sulfide (H_2S), sulfur dioxide (SO_2), cysteine (Cys), homocysteine (Hcy), and reduced glutathione (GSH), play a crucial role in modulating the environment and sustaining the dynamic equilibrium of redox reactions.[81–83] The pathophysiological progression, including FPT and inflammation, has been shown to involve dynamic interplay between polarity and RSS levels.[84,85] To elucidate the spatiotemporal correlation of two biomarkers, there is an urgent need for probes capable of simultaneous dual-parameter quantification of polarity and RSS.

Intracellular H_2S and viscosity/polarity are closely related to various physiological/pathological processes, making them possible markers for numerous diseases. In 2023, Mu *et al.*[86] reasonably developed a multifunctional fluorescent probe, HNA (Fig. 3(a)), targeting mitochondria for the cascade detection of H_2S and polarity, as well as the detection of mitochondrial DNA (mtDNA). HNA was a linear molecule with the D–π–A structure. When tightly bound to DNA grooves, its TICT effect was limited, and significant enhancement of red fluorescence (668 nm) was observed, achieving the determination of mtDNA. In addition, when H_2S reduced the azide group to $-NH_2$, HNA released the product HNAP, exhibiting orange–red fluorescence emission (604 nm). More interestingly, due to the ICT effect of HNAP, it exhibited high sensitivity to polarity, and the fluorescence emission of HNAP was blue-shifted towards the green region with decreasing polarity. HNA has successfully achieved the monitoring of polarity, H_2S, and mtDNA in live cells through fluorescence imaging. In addition, HNA could recognize the release of mtDNA in damaged mitochondria, confirming that H_2S could protect mtDNA integrity and alleviate inflammation. Therefore, this report provides new insights into the study of mitochondrial polarity and DNA dynamics.

Fan's group[84] reported a NIR fluorescent probe, MQA–DNP, for the simultaneous detection of H_2S and viscosity/polarity in mitochondria at different emission channels. As depicted in Fig. 3(b), MQA–DNP had a typical D–π–A structure, introducing *N*,*N*-dimethylamine as the electron donor, the quinoline cation unit as the electron acceptor and mitochondrial targeting group. 2,4-Dinitrophenyl (DNP) ether functioned as the specific site for recognizing H_2S, releasing the intermediate MQA, exhibiting enhanced green fluorescence emission. In addition, due to its distorted TICT state and ESICT property, the probe demonstrated a considerable degree of sensitivity towards polarity and viscosity fluctuation, which manifested as fluorescence enhancement at 714 nm in a high viscosity environment and emission at 786 nm in low polarity media. In view of its excellent spectral properties, MQA–DNP was further used to reveal the changes in H_2S, viscosity, and polarity within inflammatory cells, in the context of NAFLD, and tumor tissues. In addition, MQA–DNP has successfully detected the production of H_2S in raw meat through strip experiments; this was expected to become a prospective tool for testing H_2S in a complex environmental system.

This group[87] further designed a novel probe, PDQHS (Fig. 3(c)), based on the molecular skeleton of MQA–DNP for simultaneously tracking changes in viscosity/polarity and H_2S concentration in mitochondria. The difference was that the 4-azidobenzyl group in PDQHS was selected as the recognition group for H_2S. Spectral performance testing showed that the probe was highly selective for H_2S with fluorescence emission at 632 nm and an excellent response to viscosity/polarity beyond 706 nm. PDQHS also exhibited good biocompatibility, using PDQHS; the differentiation between cancer cells and normal cells was achieved through dual channel detection of H_2S and viscosity/polarity. More importantly, PDQHS was successfully applied to visualize H_2S in live cells and tumor tissues, which provided more sensitive and reliable imaging tools for cancer prediction.

Regarding the three probes mentioned above, we could see from Fig. 3 that the final product after the reaction between the probes and H_2S was the same. The earliest reported HNA achieved the three-parameter detection of mitochondrial H_2S, polarity, and mtDNA for the first time. Its multi-parameter detection ability was the most comprehensive among the three. Subsequently reported MQA–DNP realized the specific recognition of H_2S through the ether bond of DNP and synchronously monitored the viscosity/polarity through the TICT/ESICT mechanism, which broadened its applicability to pathological models (such as NAFLD). Based on MQA–DNP, the recognition group for H_2S in PDQHS has been optimized to 4-azidobenzyl, which successfully differentiated cancer/normal cells through dual-channel imaging. Unfortunately, the three probes for detecting H_2S were based on irreversible chemical reactions and could not track the dynamic fluctuations of H_2S in real time. In the future, researchers can further develop reversible H_2S probes targeting mitochondria, and achieve spatiotemporal-resolved dynamic monitoring by combining them with photoresponsive release technology.

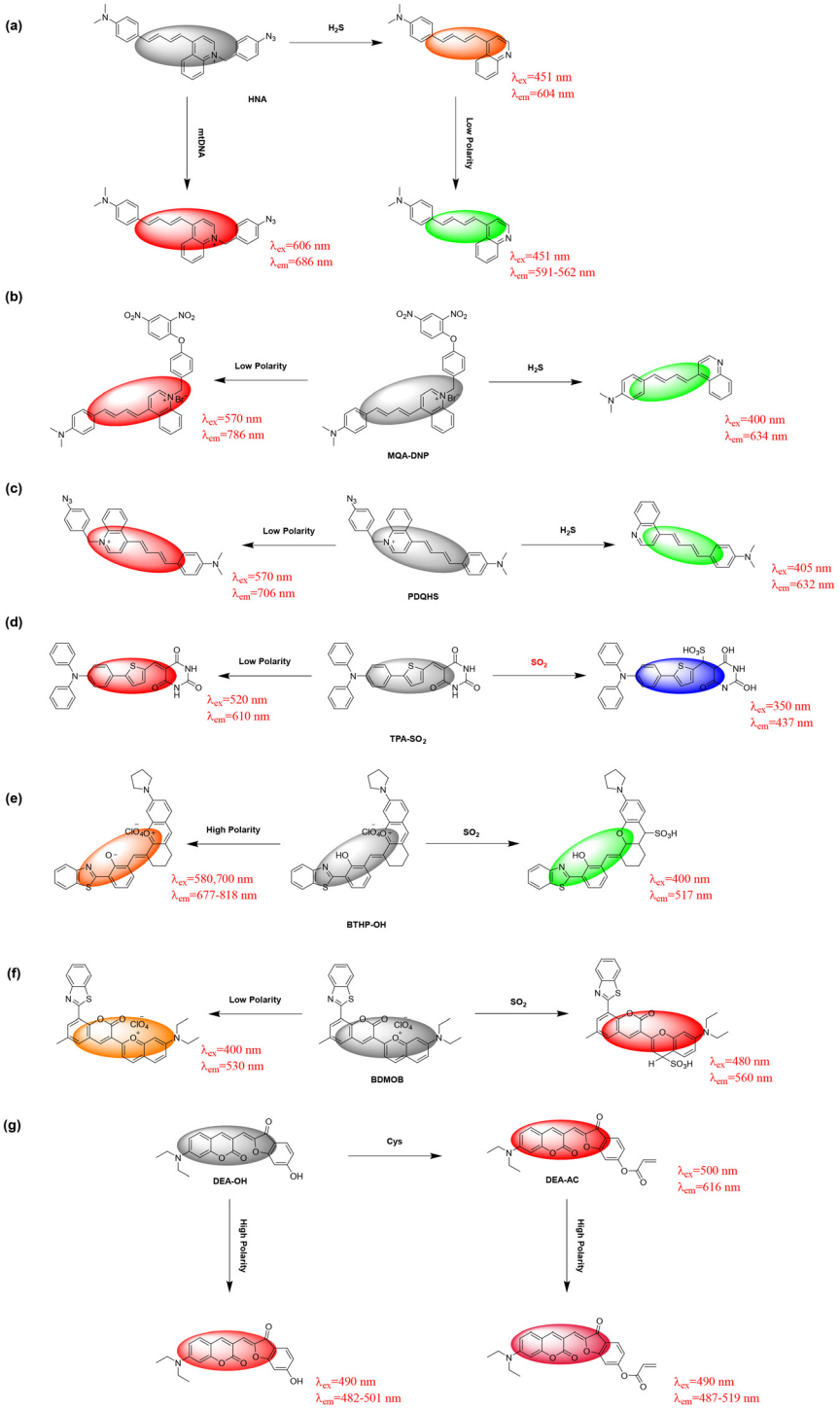

Fig. 3 Fluorescent probes for detecting polarity and RSS.

In 2022, Xie *et al.*[85] synthesized a fluorescent probe, TPA–SO_2 (Fig. 3(d)), based on TPA for detecting and imaging the polarity of LDs and the presence of SO_2 during FPT at two different channels. In TPA–SO_2, the TPA unit was selected as the fluorophore and the targeting group of LDs. Due to the ICT effect, it was sensitive to polarity and exhibited an activated fluorescence signal at 610 nm. The TPA–SO_2 probe responded to SO_2 through the Michael addition reaction of the C=C bond. When SO_2 was present, it exhibited a significant fluorescence emission at 437 nm, with a low LOD (11.9 nM) and fast response (3 min). In addition, the probe successfully achieved the visual monitoring of LD polarity and SO_2 in the constructed FPT cell model, providing a reliable means for the diagnosis and investigation of diseases associated with FPT.

In 2023, Zhang *et al.*[88] synthesized a dual-functional NIR fluorescent probe, BTHP-OH (Fig. 3(e)), based on benzopyran derivatives for the simultaneous detection of SO_2 and polarity. The emission of BTHP-OH changed from 677 nm to 818 nm as the polarity of the medium increased. After adding SO_2, the fluorescence changed from red to green, and the fluorescence intensity of I_{517}/I_{768} nm increased by about 33.6 times, reaching steady state within 1 min. Cell imaging showed that BTHP-OH could specifically target mitochondria and monitor exogenous SO_2 in A549 cells. More importantly, BTHP-OH has been successfully used for the dual channel monitoring of SO_2 and polarity in inflammatory cells and mouse models. This provides a favorable tool for pathological research on SO_2 and polarity related diseases.

In 2024, Wang *et al.*[89] created a dual-responsive fluorescent probe, BDMOB (Fig. 3(f)), to achieve the concurrent measurement of polarity and SO_2 by assembling the SO_2-responsive site based on a benzopyran derivative with a push–pull electron group. As a responsive probe for SO_2, BDMOB exhibited enhanced orange fluorescence emission accompanied by extremely high sensitivity (LOD = 0.239 μM), selectivity, and a wide suitable pH range (5–10). Meanwhile, the ICT effect of the molecular structure made it sensitive to polarity changes; with increasing polarity, it exhibited significant fluorescence enhancement in the NIR region. Given the excellent spectral performance of BDMOB, it has been used for imaging SO_2 in living cells, successfully distinguishing cancer cells from normal cells by tracking the fluctuation of SO_2. Furthermore, using LPS and RSL3 as inducers of inflammation and FPT models, BDMOB successfully monitored changes in SO_2 and polarity during these two pathological processes, which provided new insights into the field of chemical biology and related disease diagnosis.

Zhang *et al.*[90] designed and synthesized two fluorescent probes, DEA–OH and DEA–AC (Fig. 3(g)), for detecting Cys based on the coumarin–aurone skeleton. DEA-OH and DEA-AC showed good sensitivity for Cys detection through copper displacement and an acrylic ester hydrolysis mechanism with the LOD values of 7.25 μM and 1.65 μM, respectively. Among them, the DEA–AC probe had the merits of a fast response time (kinetic reaction rate constant: 0.00747 s^{-1}) and red emission for detecting Cys, and it effectively carried out the dynamic observation of Cys levels in living cells, thereby supplying a worthwhile tool for the exact sensing and tracing the fluctuation of Cys levels. In addition, the fluorescence emission of the two probes exhibited a linear correlation with the polarity of the solvent within an ET (30) range spanning from 30 to 65 kcal mol^{-1}. This manifestation suggested their capability to detect and monitor fluctuations in the polarity of the surrounding environment. Unfortunately, no biological applications for polarity monitoring were developed for the probes.

Polarity and $ONOO^-$

Peroxynitrite ($ONOO^-$), which is produced by the reaction of highly active nitric oxide (NO) and the superoxide anion ($O_2^{\bullet-}$), belongs to the category of reactive nitrogen species (RNS).[91,92] It has strong oxidative and nucleophilic properties and can participate in various biochemical reactions in organisms.[93] $ONOO^-$ plays an important role in cellular oxidative stress, inflammation and immune response.[92] A high concentration of $ONOO^-$ can trigger damage to DNA and organelles, and even apoptosis, through various signaling pathways. These changes can further trigger the onset of diseases such as tumors, diabetes, cardiovascular diseases, and neurodegenerative diseases. Therefore, quantitative monitoring of $ONOO^-$ in living organisms is essential. The design mechanism of the probes for polarity and $ONOO^-$ response described below belongs to the type illustrated in Fig. 4.

Liu *et al.*[94] designed and assembled a super-resolution imaging probe, CPC (Fig. 5(a)), suitable for subcellular component detection based on the coumarin–phenylhydrazine–carboxyl group. This probe could simultaneously monitor the distribution of $ONOO^-$ and polarity in mitochondria and LDs, and the response of CPC to polarity was characterized by a "turn-on" fluorescence signal, while the response to $ONOO^-$ was the opposite. CPC exhibited excellent imaging capability under structured illumination microscopy; by using CPC, it was observed that the polarity of LDs increased and their morphology became more contracted during FPT, indicating the physical transition of intracellular LDs from heterogeneity to homogeneity. In addition, the accumulation of $ONOO^-$ in mitochondria led to mitochondrial oxidative stress, triggering LDs' dysfunction and decoupling between mitochondria and LDs. In summary, this toolkit will become a powerful tool for examining subtle changes in multiple organelle interactions.

The aberrant mitochondrial microenvironment is strongly correlated with mitochondrial and cellular dysfunction. To this end, in 2023, Huang *et al.*[95] synthesized a multifunctional fluorescent probe, DPB (Fig. 5(b)), targeting mitochondria that reacted to polarity, viscosity, and $ONOO^-$ by integrating several response moieties with a single fluorophore. The probe had a classic D–π–A structure; the pyridine group bearing a positive charge played the role of specifically targeting mitochondria. Its TICT property enabled it to show a response towards polarity and viscosity, and phenylboronic acid ester served as a recognition group for $ONOO^-$. Specifically, as the polarity underwent an upward trend, the fluorescence intensity of DPB at 470 nm sharply declined. In contrast, the fluorescence emission of DPB at 658 nm rose as the viscosity increased, yet it diminished as the concentration of $ONOO^-$ increased. Subsequently, the DPB probe was used for imaging in the living cells, successfully monitoring fluctuation in mitochondrial polarity, viscosity, and endogenous/exogenous $ONOO^-$.

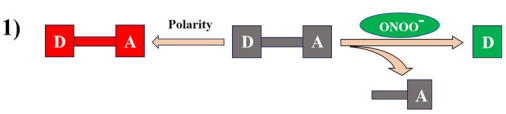

Fig. 4 The fluorescence detection mechanism of probes for polarity and $ONOO^-$.

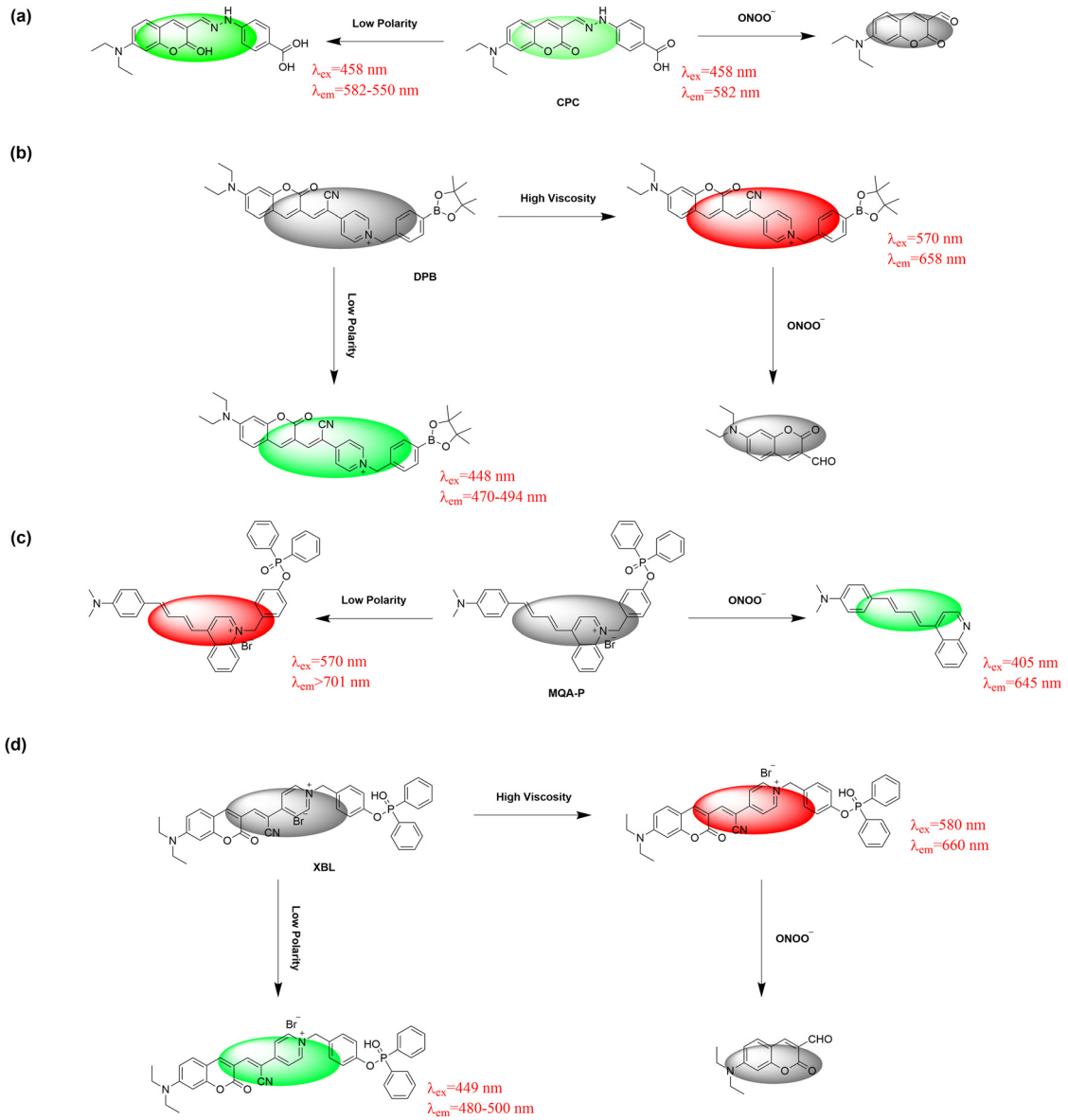

Fig. 5 Fluorescent probes for detecting polarity and $ONOO^-$.

DPB exhibited pronounced fluorescence intensity within cancer cells that featured low polarity and elevated viscosity, enabling the precise identification of cancer cells at the level of multiple biomarkers. This holds significant promise for the investigation of the mitochondrial microenvironment and the diagnosis of cancer. The same year, Fan's group[96] proposed an NIR fluorescent probe, MQA–P (Fig. 5(c)), for the simultaneous detection of $ONOO^-$, viscosity, and polarity within mitochondria. The typical D–π–A structure of the probe gave it active ESICT characteristics, exhibiting a significant optical change with changes in polarity. In addition, the TICT property made MQA–P sensitive to viscosity changes. The diphenylphosphonic acid ester unit acted as a recognition group for $ONOO^-$, and upon interaction with $ONOO^-$, it released the intermediate MQA, thereby weakening the ICT effect and causing a blue-shift in fluorescence emission. Specifically, the probe exhibited a significant turn-on response at 645 nm to $ONOO^-$, and exhibited a high level of sensitivity towards viscosity and polarity within the NIR channel, in which the emission wavelength (λ_{em}) exceeded 704 nm. Using MQA–P, this work revealed that FPT induced by erastin was accompanied by a significant upregulation of $ONOO^-$ and an increase in viscosity (or a decrease in polarity). In addition, the simultaneous use of $ONOO^-$, viscosity, and polarity for cancer diagnosis has been successfully achieved at the cellular/tissue level and in a tumor mouse model, which has great potential for preclinical research, medical diagnosis, and image-guided surgery.

In 2024, Li *et al.*[97] managed to synthesize the XBL probe (Fig. 5(d)), targeting mitochondria based on TICT and ICT mechanisms, which was used to monitor the dynamic changes

in viscosity, polarity, and $ONOO^-$. Similar to the MQA–P structure, cationic pyridine was used as the targeting unit for mitochondria, and the diphenyl phosphate group served as the recognition unit for $ONOO^-$. In addition, compared with DPB, in the structural design of XBL, a coumarin derivative was also used as the fluorophore, achieving dual-channel emission, and they adopted the D–π–A architecture and utilized the ICT and TICT mechanisms to respond to polarity and viscosity. The findings of a specific experiment indicated that, as the viscosity diminished or the concentration of $ONOO^-$ increased within 2 min, there was an increase in the fluorescence intensity at 660 nm, showing a fast response to $ONOO^-$ while the fluorescence intensity around 480–500 nm declined as the polarity increased. Based on the timely monitoring of cellular viscosity, polarity, and $ONOO^-$, the probe successfully distinguished normal cells from cancer cells using fluorescence imaging. In addition, imaging results also indicated that the FPT process was accompanied by changes in polarity and viscosity, and in the mouse inflammation model, viscosity increased. Therefore, this probe could provide a chemical means for understanding the physiological alterations and pathological modifications in diseases.

Based on the above discussion, it was obvious that the probes DPB, MQA–P, and XBL formed a "toolbox" with complementary functions through differentiated detection mechanisms (TICT/ESICT/NIR), wavelength coverage (visible light/NIR), and application scenarios (cancer, ferroptosis, inflammation). Their coordinated use can comprehensively analyze the complex interaction network of polarity, viscosity, and oxidative stress in the mitochondrial microenvironment, providing multi-dimensional solutions for research on disease mechanisms and precise diagnosis and treatment. In the future, the design of probes can draw on their complementary advantages, further integrate dynamic responses, multimodal imaging, and intelligent analysis technologies, and promote the leap of chemical biology towards systems medicine.

Polarity and pH

Intracellular pH and polarity, as two important microenvironments, are closely related to the development of many diseases.[98,99] For example, the tumor microenvironment (pH 6.5–7.0) and abnormal membrane polarity synergistically promote drug resistance and metabolic reprogramming.[100,101] In AD, the generation of Aβ aggregates is strongly correlated with a decrease in local pH and polarity.[102,103] In addition, pH and polarity jointly regulate enzyme activity, membrane protein conformation, nutrient transport, and signal transduction.[4] Therefore, the development of probes that can simultaneously detect polarity and pH is of great significance for revealing the dynamic coupling mechanism of the microenvironment and promoting innovation in precision diagnosis and treatment technology.

In 2021, based on the mitochondrial microenvironment (high pH value (>7.0) and low polarity) as an input, a mitochondrial membrane potential (MMP) responsive AND logic gate fluorescent probe, A, was designed by Liang's group.[104] As displayed in Fig. 6(a), probe A used coumarin as the molecular skeleton, which was hydrolyzed under alkaline conditions to generate a coumarin acid derivative with an ICT effect and sensitivity to polarity changes. Specifically, probe A exhibited bright fluorescence emission under low polarity and high pH conditions. In addition, the pyridine moiety carrying a positive charge provided targeted selectivity for cancer cells with high MMP. Fluorescence imaging results indicated that the fluorescence intensity of probe A in cancer cells and tumor tissues was indeed 51.9-fold higher than that of the normal control group, which would provide a certain technical basis for early cancer diagnosis.

In 2021, Thomas *et al.*[105] exploited a novel membrane probe, ND6 (Fig. 6(b)), utilizing the 1,8-naphthalimide fluorophore. In terms of the molecular structure, protonation of the ND6 head group was closely related to pH changes and further affected fluorescence emission. When the pH dropped from 7.4 to 6 or below, the fluorescence of ND6 almost doubled. The photophysical performance measurements and quantum chemical theory calculations further verified the sensitivity of ND6 to polarity and pH changes. In addition, ND6 had a higher membrane affinity, and molecular dynamics simulation also confirmed its incorporation and interaction behavior with membrane lipids. Through fluorescence imaging, the probe exhibited membrane-bound properties in cancer cell lines (MCF7), cancer spheroids (MDA-MB-468), and hippocampal neurons. The use of ND6 to label nerve endings during the transport of synaptic vesicles revealed the role of cholesterol in recombinant synaptic vesicles. Overall, this probe holds significant promise for investigating membrane dynamics and synaptic function not only in neurons but also in various other secretory cells and tissues. In 2022, a fluorescent probe with phenothiazine quinoline (PTZ-Q) (Fig. 6(c)) as the molecular skeleton was designed by Zahrani.[106] Due to its typical D–A structure, the probe exhibited an ICT effect and sensing property for polarity and pH changes. UV and fluorescence spectra indicated that as the solvent polarity increased, the Stokes shift of the probe increased, and the fluorescence emission shifted towards longer wavelength; when the solvent pH changed, PTZ-Q exhibited reversible colorimetric and fluorescence changes. PTZ-Q has been successfully used to create colorimetric and fluorescent test strips for detecting changes in the pH of a medium. Regrettably, the probe has not been used further to explore biological applications related to polarity and pH.

In 2022, a group of fluorescent oxazolidine derivatives containing hydroxyl and naphthalene functional groups were synthesized by Razavi *et al.*[107] and used for pH and polarity monitoring (Fig. 6(d)). UV and fluorescence spectroscopy detection showed that the color and fluorescence intensity of the probes varied depending on the hydroxyl and naphthalene functional groups substituted on the conjugated oxazolidine. Therefore, this work developed colorimetric and fluorescent chemical sensors based on these probes for monitoring the pH and polarity of the medium.

In 2023, a series of fluorescent probes based on benzothiazole derivatives (HTBs) (Fig. 6(e)) were prepared by Hong *et al.*[108] Spectral testing showed that the probes exhibited

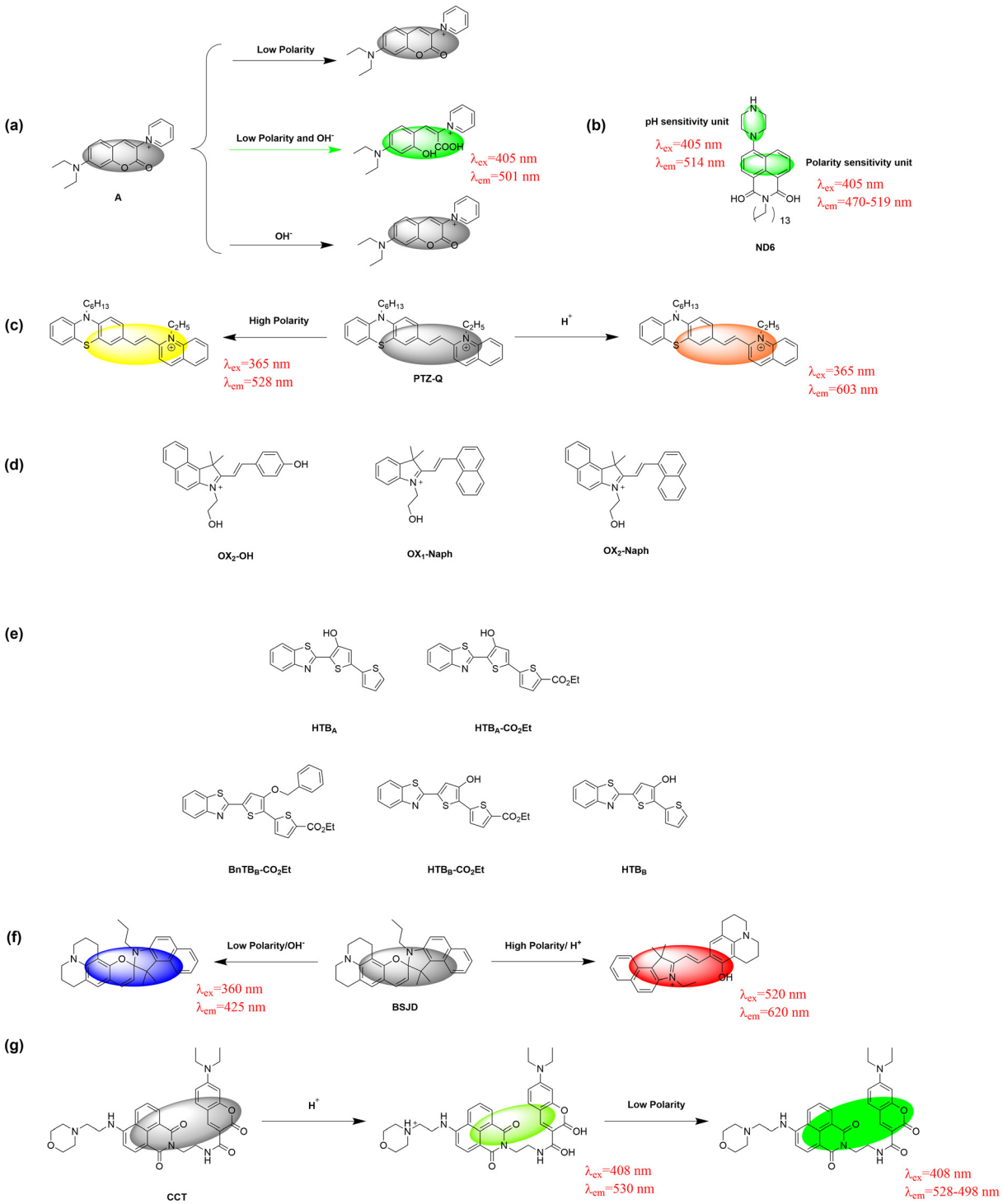

Fig. 6 Fluorescent probes for detecting polarity and pH.

bright green or orange emission due to deprotonation of the hydroxyl group under high pH conditions. In addition, due to the ESIPT and ICT effects in the molecular structure, all HTB derivatives displayed bright fluorescence emission in low polarity solvent. Cell imaging experiments showed that HTBA could selectively stain alkaline mitochondria. On the other hand, HTBB–CO_2Et was successfully used to stain LDs in living cells. Overall, the results of this study indicated that changes in substituents in HTB molecules led to significant changes in their intracellular localization and imaging capability, providing new ideas for further expanding fluorescent probes targeting various organelles.

The main feature of early atherosclerosis (AS) is the formation of foam cells (FCs), which are characterized by abnormal accumulation of LDs and lysosomal dysfunction.[109,110] Therefore, in order to study the pathological processes related to AS, in 2024, a fluorescent probe, BSJD (Fig. 6(f)), was engineered by Li *et al.*[111] Leveraging its sensitivity to both polarity and pH levels, BSJD was intended to realize the dual-color imaging of LDs and lysosomes. The spiropyran in the BSJD structure could undergo isomerization between open and closed ring forms, which was reversibly regulated by fluctuations in pH and polarity. Specifically, under acidic or strongly polar conditions, the BSJD probe was in the positively charged open ring form with an extended π-conjugated system, resulting in redshifted absorption and fluorescence spectra. In addition, the presence of $-NH_2$ in BSJD enabled it to locate the lysosome. However, under converse conditions, BSJD existed in a closed loop configuration, the ICT process was inhibited, fluorescence emission underwent a blueshift, and BSJD tended to target neutral and low polar LDs. The photophysical property at different pH values and in polar solvents validated the above design concept. The cell imaging results indicated that BSJD could be used to observe in real-time early activation and later inhibition of lipophagy during FC formation, and also demonstrated the important role of lipophagy in regulating lipid metabolism and alleviating FC formation. In addition, BSJD successfully achieved the visualization of FC plaques in AS mice with rapid pharmacokinetics. BSJD was anticipated to become a beneficial method for early discernment and monitoring of AS diseases.

In 2024, based on ICT and PET mechanisms, Chao *et al.*[101] designed a fluorescent probe, CCT (Fig. 6(g)), that responded to pH and polarity. Due to the PET effect between morpholine and naphthalimide in the molecular skeleton, the CCT probe was sensitive to pH. Specifically, the protonation of the nitrogen atom in the morpholine moiety could block the PET process, resulting in the bright fluorescence emission of CCT at 530 nm. In contrast, deprotonation under alkaline conditions led to the PET effect and fluorescence reduction. In addition, the presence of polarity sensitive units (coumarin and naphthalimide) caused CCT to emit strong and long wavelength fluorescence in low polarity media. And when the probe was under low pH and polarity conditions, the fluorescence intensity was stronger than that under any single condition. In addition, the photostability and anti-interference experiments showed that the probe had excellent photostability and high selectivity for polarity and pH. Based on the above features, the probe was further used in cell imaging. Due to the low pH and polarity environment of cancer cells, the probe successfully distinguished between cancer cells and normal cells, indicating its potential for early cancer diagnosis.

Polarity and viscosity

Intracellular polarity and viscosity are critical for the establishment of cellular homeostasis, and are important indicators of emerging pathology in the cellular environment.[1,9] Viscosity has a significant effect on many cellular motions, including biomolecule interactions, cellular metabolism, signal transduction, energy transport *etc.*[112,113] Polarity shows a dynamic trend during cellular movements such as membrane fusion, protein folding, and peptide aggregation. Abnormalities in viscosity and/or polarity cause an imbalance in the stable internal environment of cells, metabolic disorder, and even diseases such as inflammation, cancer, and cardiovascular diseases.[114–116] Therefore, the development of methods to simultaneously monitor changes in viscosity and polarity is important for understanding the etiology of related diseases and their treatment. The design mechanism of the probes for polarity and viscosity responses described below belongs to the type illustrated in Fig. 7.

The change in the microenvironment within LDs can affect various physiological processes such as lipid metabolism, protein degradation, and signal transduction.[117–119] In 2022, Han *et al.*[120] synthesized two ICT-based fluorescent probes targeting LDs, LDP-1 and LDP-2 (Fig. 8(a)). The results of photophysical performance testing showed that these two probes were sensitive to both medium polarity and viscosity, and their emission wavelengths were longer than 600 nm in different environments. They had good selectivity and excellent biocompatibility. The PCC for LDs in HeLa cells was 0.97 and 0.89, indicating that the two probes could specifically track LDs in HeLa cells.

Wang *et al.*[121] constructed a fluorescent probe, Couoxo–LD (Fig. 8(b)), which was designed on the basis of a coumarin fluorophore, which responded to polarity and viscosity. The introduction of coumarin into Couoxo–LD increased its lipophilicity, and the typical D–π–A structure gave it TICT characteristics, which showed bright fluorescence emission in low polarity and high viscosity media. Therefore, the probe successfully lit up intracellular LDs (PCC = 0.93). By altering the external environment, Couoxo–LD could be used to distinguish changes in LD polarity in live and dead HeLa cells. In addition, the excellent selectivity and good biocompatibility of Couoxo–LD further enabled its successful application in imaging LDs in zebrafish.

Duangkamol *et al.*[122] crafted a collection of fluorescent probes that were developed on the basis of the coumarin skeleton, in which LD–PYR (Fig. 8(c)) exhibited high sensitivity to polarity and viscosity due to the TICT effect, specifically, a redshift of LD–PYR was displayed from 556 nm to 585 nm with increasing polarity from hexane to EtOH. It exhibited high fluorescence intensity at 480–490 nm in viscous media. In addition, LD–PYR had a specific targeting ability for low polarity and high viscosity LDs, and achieved success in separating cancer cells from non-cancer cells.

Fig. 7 The fluorescence detection mechanism of probes for polarity and viscosity.

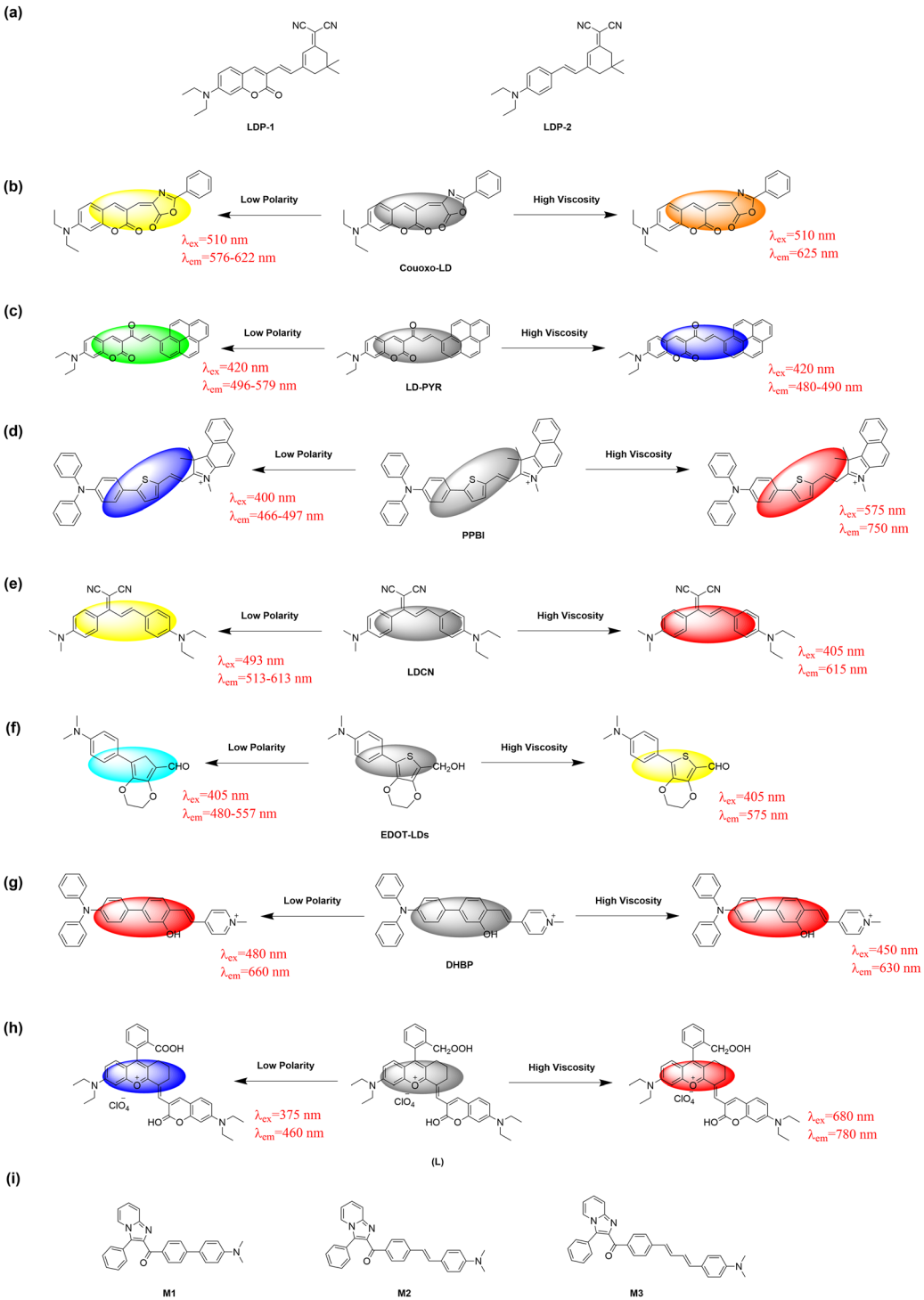

Fig. 8 The fluorescent probes employed to detect polarity and viscosity.

Overall, both Couoxo–LD and LD–PYR were fluorescent probes based on TICT/ICT mechanisms for detecting polarity and viscosity, with coumarin as the fluorophore. However, LD–PYR achieved a higher selectivity and the AIE enhancement effect through the introduction of the pyrene unit, while Couoxo–LD was characterized by its simple synthesis and broad-spectrum response. In the future, researchers can further optimize the structure of probes: (1) probes with high sensitivity and targeting ability can be developed by combining the broad-spectrum response of Couoxo–LD with the AIE properties of LD–PYR; (2) the penetration depth of *in vivo* imaging can be increased by replacing the pyrene unit of LD–PYR with

a near-infrared (NIR) fluorophore, thus promoting the clinical transformation of the monitoring tools for the LD microenvironment.

In 2023, Wang *et al.*[123] developed a polarity and viscosity dual responsive fluorescent probe, PPBI (Fig. 8(d)), that could target mitochondria and LDs. PPBI used TPA as a fluorophore and exhibited TICT and AIE effects, which displayed excellent specificity in response to polarity and viscosity. In addition, the probe achieved the recognition of cancer cells through fluorescence imaging in red and green fluorescence channels, and successfully visualized changes in the cell microenvironment in inflammation and FPT models. More importantly, in the alcohol induced acute liver injury mice model, the probe could effectively detect the therapeutic effect of drugs by responding to changes in polarity and viscosity. This report provided a promising strategy for biological imaging and medical diagnosis.

Wang's group[124] constructed a TICT probe, LDCN, with a D–A–D structure using malononitrile as the electron acceptor, and diethylamino and dimethylamino groups as the donor, as depicted in Fig. 8(e). LDCN exhibited sensitivity to polarity and viscosity, and could target LDs. Spectral testing showed that LDCN possessed outstanding selectivity, favorable photostability, and a substantial Stokes shift (114 nm) in response to polarity and viscosity. In addition, LDCN displayed outstanding targeting ability towards LDs in HeLa cells and tobacco seedling leaf cells, with PCC as high as 0.91 and 0.85, respectively. The findings suggested that the probe was capable of selectively detecting LDs within living cells. In addition, based on the response of LDCN to viscosity during beverage spoilage, LDCN achieved the detection of freshness of beverages.

In 2024, a fluorescent probe, EDOT–LDs, based on the ICT effect for viscosity and polarity responses was reasonably designed by Chao *et al.*[125] As shown in Fig. 8(f), this probe used dimethylamino as an electron donor and also served as a targeting unit for LDs. The excellent photostability and low cytotoxicity enabled EDOT–LDs to be further used in cell imaging. In cells maintained under starvation conditions or stimulated by oleic acid, the number of bright fluorescent LDs decreased or increased dynamically, signifying that the probe had the capacity to monitor dynamic changes to LDs in cells. Furthermore, the probe also achieved the visualization of viscosity changes in cells and zebrafish, providing a new perspective for studying polarity and viscosity changes in organisms.

Bian *et al.*[126] also developed a fluorescent probe, DHBP (Fig. 8(g)), that was sensitive to polarity and viscosity in dual channels through a similar strategy. The probe exhibited excellent selectivity towards viscosity and polarity *in vitro* and *in vivo*. As the polarity decreased, the green fluorescence signal was significantly enhanced, and the synergistic effect of viscosity and polarity made the red fluorescence signal more sensitive. The fluorescence imaging results showed that the probe successfully detected polarity and viscosity changes in LPS induced inflammatory cells and mice. In addition, DHBP realized the visualization of viscosity and polarity changes in mice with liver injury caused by diabetes, and it was further utilized to evaluate the therapeutic effect of drugs.

Zhang *et al.*[127] devised a novel dual-channel fluorescent probe (L) (Fig. 8(h)) with the intention of detecting polarity and viscosity. The typical D–π–A structure of the probe enabled it to exhibit the TICT effect. When it was in a high viscosity environment, TICT was blocked and the probe emitted bright NIR fluorescence at 780 nm. Meanwhile, due to the presence of the polar-sensitive coumarin unit, the probe exhibited polarity-dependent fluorescence emission at 460 nm. In addition, the good biocompatibility of probe L allowed it to be further used for cells and *in vivo* imaging. The successful recognition of cancer cells in dual channels and *in vivo* imaging of rheumatoid arthritis (RA) in mice was achieved through fluorescence imaging of polarity and viscosity changes using the probe.

Zhu *et al.*[128] created three fluorescent probes with the D–A configuration, M1–M3 (Fig. 8(i)), based on imidazopyridine, all of which exhibited sensitivity to polarity and viscosity. The polarity or viscosity dependent behavior of M1–M3 was adjusted based on the different conjugated lengths of the molecules. In addition, due to the PET mechanism being activated when 2,6-dichloro-4-nitroaniline (DCN) was bonded to M1–M3 in THF, the fluorescence of the probes was quenched, thereby achieving highly sensitive detection of DCN with LODs of 189 ppb, 62 ppb, and 54 ppb, respectively. This not only provided new tools for the detection of DCN pesticide, but also offered new ideas for studying biological processes related to viscosity and polarity.

Polarity and Aβ

AD is a frequently occurring neurodegenerative illness.[129] Senile plaques (SPs) and neurofibrillary tangles (NFTs) are the two main pathological features of AD, composed of β amyloid (Aβ) aggregates and hyper-phosphorylated tau protein, respectively.[130,131] The design mechanism of the probes for polarity and Aβ response described below belongs to the type illustrated in Fig. 9. The selective differentiation between Aβ and tau protein was crucial for the study of the AD pathological process.[131] For this purpose, Kim's research group[132] developed three polar-sensitive probes based on a benzimidazole derivative for the detection and differentiation of Aβ and tau protein. These probes possessed an ICT effect and exhibited multi-color fluorescence emission influenced by changes in solvent polarity. Due to the difference in the microenvironment of Aβ and tau aggregates, BZ2 and BZ3 (Fig. 10(a)) exhibited selective binding to two proteins at different emission wavelengths *in vitro*. Unfortunately, this work did not

Fig. 9 TThe fluorescence detection mechanism of probes for polarity and Aβ.

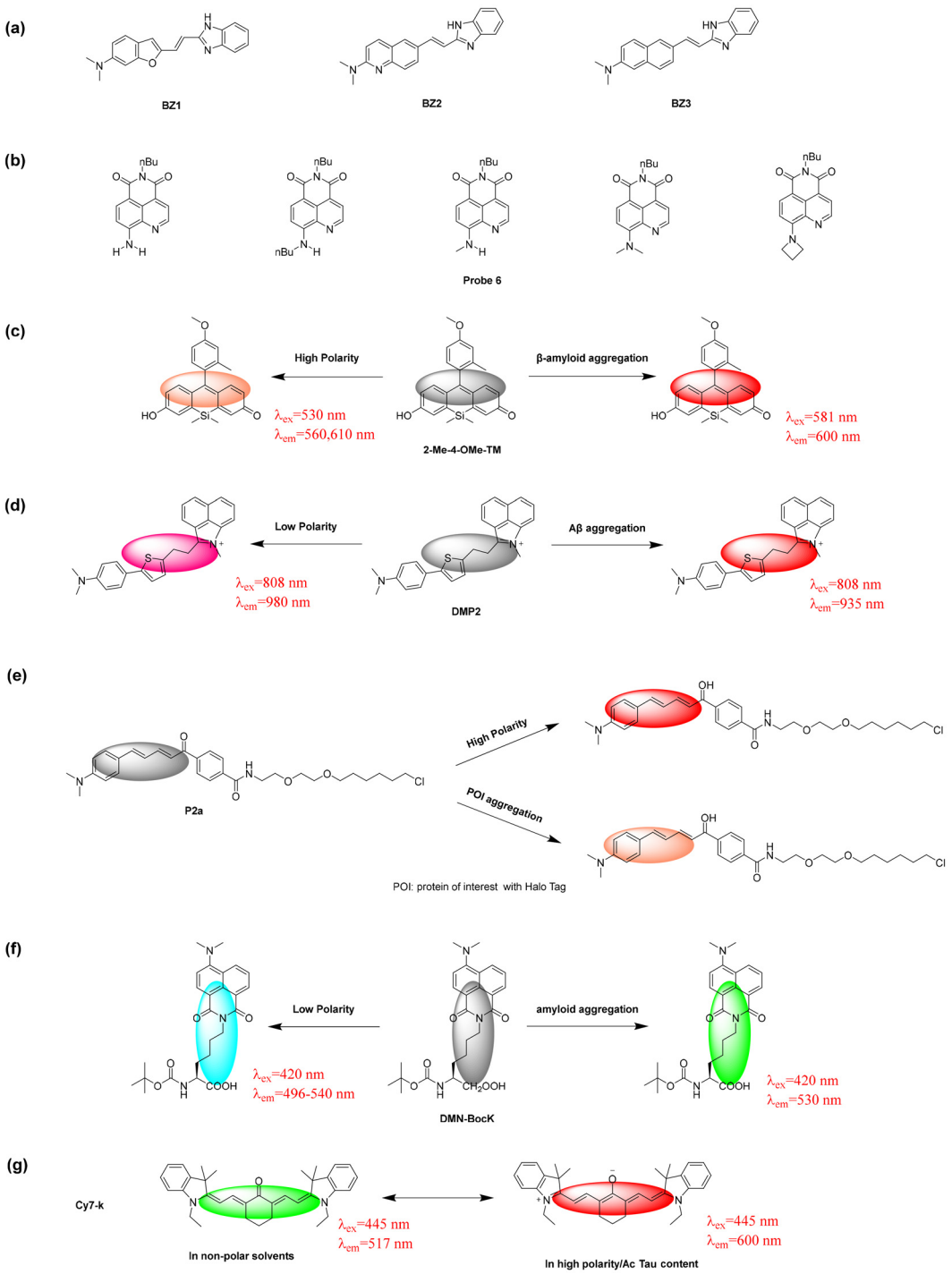

Fig. 10 Fluorescent probes for detecting polarity and Aβ.

investigate the selective differentiation of Aβ and tau protein *in vivo*.

Herranz *et al.*[133] created a range of quinolimide-based fluorescent probes for detecting amyloid protein aggregation. These probes had a classic D–A electronic structure, were remarkably sensitive towards polarity, and had long fluorescence lifetimes in a hydrophobic environment, indicating their excellent properties for the detection of amyloid protein fibrotic aggregation. The fluorescence emission of probe 6 (Fig. 10(b)) was enhanced by 11 times in the presence of Aβ aggregates, and with prolongation of the aggregation time, the maximum emission was blue-shifted by 63 nm. When Aβ aggregates were present, FLIM and ratio imaging were performed on probe 6 using one-photon excitation or TPE, suc-

cessfully identifying different types of aggregates and their changes over time. In addition, in the neurotoxin MPTP (1-methyl-4-phenyl-1,2,3,6-tetrahydropyridine)-induced zebrafish model with neuronal injury, the probe successfully visualized amyloid protein aggregates.

The initial stage of Aβ oligomerization in AD is crucial for tracing the origin of the disease. Hence, in 2022, Espinar-Barranco *et al.*[134] proposed a polarity sensitive fluorescent dye, 2-Me–4-OMe–TM (Fig. 10(c)) (a silicon modified xanthene derivative), for the real-time detection of polarity fluctuations during the initial phase of Aβ aggregation. The dye exhibited a dual emission property, and the ratio of the average fluorescence lifetimes between two channels was used as a scale of polarity changes. Through steady-state, time-resolved fluorescence spectroscopy, and FLIM techniques, the dye successfully detected early polarity changes in the formation process of Aβ aggregates and established a method for discriminating different types of aggregates. The advantage of this method was non-invasive and independent of the concentration of the dye.

In 2023, Miao *et al.*[135] reported a series of NIR-II fluorescent probes for responding to Aβ plaques. This series of probes all used carbazole with a positive charge as an electron acceptor and had a typical D–π–A structure. Photophysical analysis showed that DMP2 (Fig. 10(d)) had an excellent spectral performance and was further used in research related to Aβ plaques. After binding to Aβ plaques, the NIR-II fluorescence of DMP2 increased by 48 times due to its suppressed TICT effect. In addition, DMP2, with its small molecular weight and lipophilicity, could achieve ideal deep-tissue penetration through the blood–brain barrier (BBB) and in the NIR-II region, and its response to Aβ plaques could still be detected even in 1.5 cm thick chicken tissue. Even more interestingly, DMP2 successfully achieved specific imaging of Aβ plaques in AD mice.

Protein homeostasis is of great significance in the normal operation of many physiological processes,[136] and disruption of the protein balance caused by external environmental factors can lead to protein misfolding or aggregation.[137] Therefore, Yang *et al.*[138] developed a chalcone-based probe (Fig. 10(e)) that was sensitive to both polarity and viscosity to monitor the protein aggregation process. When the probe bound to the target protein, it exhibited a "gradual turn-on" fluorescence performance, and the emission wavelength varied for different aggregation periods of the protein, thus enabling the study of microenvironmental changes throughout the protein aggregation process. Finally, through fluorescence imaging, the probe achieved success in visualizing the protein aggregates that were triggered by proteasome inhibitors within living cells. This work initiated a new avenue for studying the physiological and pathological processes related to protein aggregation.

In 2024, Gamez's group[139] reported a polarity sensitive probe, DMN–BocK (Fig. 10(f)), based on a DMN functionalized lysine residue for detecting the amyloid protein aggregation process in diseases such as AD/PD. The probe was connected to lysine protected by water-soluble *tert*-butyloxycarbonyl (Boc) and 4-*N*,*N*-dimethylaminonaphthalimide (4-DMN), where the presence of lysine increased the water solubility of DMN–BocK and allowed it to be incorporated into the peptide sequence, thereby yielding more conformational information on the amyloid protein. A polarity-sensitive unit (DMN) made the emission of DMN–BocK solvatochromic; by using this property, the probe could detect subtle polarity changes within a range of different amyloid protein binding sites, such as Aβ and tau, alpha synuclein, and non-mammalian/mammalian prions. Meanwhile, DMN–BocK successfully monitored the aggregation process of amyloid protein *in vitro* and bacteria through fluorescence imaging.

Recently, a polarity sensitive ratiometric fluorescent probe, Cy7–K (Fig. 10(g)), based on cyanine was developed by Wang's research group.[140] Unlike molecules with typical ICT effects, this probe was a neutral molecule and exhibited higher fluorescence efficiency in high polarity solvents than in low polarity solvents. Using ratiometric fluorescence imaging of the probe, it was clearly observed that Aβ could increase the content of acetylated tau protein (AC Tau) by inhibiting the expression of histone deacetylase 6, and the polarity was highly correlated with AC Tau, ultimately leading to enhanced cell polarity. In addition, the Cy7–K probe was able to successfully penetrate the BBB, imaging polarity differences in different brain regions, and it was used to distinguish APP/PS1 mice from wild-type mice, indicating the potential application of this probe for real-time tracking of AD occurrence and development.

Polarity and HSA

Human serum albumin (HSA) is one of the most abundant proteins containing thiol in the blood, involved in maintaining blood osmotic pressure and transporting fatty acid, metabolites, and various drugs.[141–143] It plays an important role in many physiological processes. The design mechanism of the probes for polarity and HSA responses described below belongs to the type illustrated in Fig. 11. Besides, the probes for HSA and polarity discussed below are shown in Table 1.

In 2020, a TPA-based NIR probe L with the TICT effect was designed by Yang's group.[16] Probe L could selectively bind to HSA/BSA and emit bright fluorescence at 668 nm. At the same time, the probe was sensitive to polarity and emitted bright green fluorescence in low polarity media, which could specifically target LDs in the green channel. By binding L with albumin protein, the location of sentinel lymph nodes in the mouse model could be determined. In addition, probe L suc-

Fig. 11 The mechanism of detecting polarity and HSA fluorescent probes for detecting HSA.

Table 1 Fluorescent probes for detecting polarity and HSA

Probe structure	Polarity		HSA			Biomedical application
	λ_{ex}	Range of emission	λ_{ex}	λ_{em}	Response time	
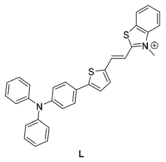 L	430 nm	507–460 nm	561 nm	668 nm	2 h	Locating sentinel lymph node in mouse model
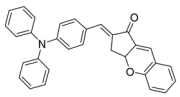 TPA-CPO	485 nm	566–602 nm	485 nm	610 nm	15 min	Imaging HSA in HeLa cells
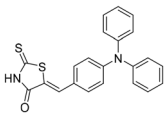 DPAR	488 nm	549–606 nm	514 nm	575 nm	4 min	Detecting HSA in actual urine samples and targeting LDs
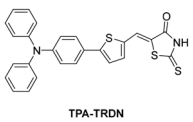 TPA-TRDN	497 nm	575–641 nm	497 nm	610 nm	10 min	Detecting HSA in actual urine samples and recognizing cancer cells
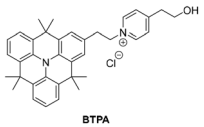 BTPA	470 nm	654–757 nm	470 nm	650 nm	<30 s	Detecting HSA in human urine samples
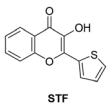 STF	37 0 nm	408–427 nm	400 nm	515 nm	<10 s	Timely detection of HSA in serum samples
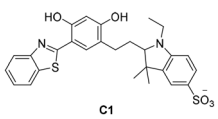 C1	380 nm	466–600 nm	380 nm	446 nm	—	Measuring HSA in human blood on a test strip

cessfully distinguished cancer cells from normal cells in the green fluorescence channel.

In 2021, Zhang's group[144] also developed a TPA-based HSA fluorescent probe, TPA–CPO. This probe featured a characteristic D–π–A structure and demonstrated sensitivity towards polarity. The maximum emission wavelength underwent a "redshift" with increasing solvent polarity. When it bound to HSA, the TICT effect was suppressed, and the probe exhibited bright fluorescence enhancement at 610 nm. The probe had a large Stokes shift (134 nm), low LOD (13.65 mg mL^{-1}), and a wide linear range (0.30–3.65 mg mL^{-1}) for detecting HSA. In addition, TPA–CPO successfully achieved the imaging of HSA in HeLa cells.

In 2022, the research group reported a fluorescent probe, DPAR,[145] for the quantitative detection of HSA by altering the receptor structure of TPA–CPO. Compared with TPA–CPO, DPAR had higher sensitivity for detecting HSA (LOD = 0.98 mg mL^{-1}), and it was also successfully used for the visual monitoring of HSA in live cells. Furthermore, it achieved the detection of HSA in actual urine samples. In addition, DPAR was also sensitive to polarity, and through the targeting of low polarity LDs, DPAR achieved the recognition of cancer cells. In the same year, the group also designed a polarity sensitive fluorescent probe, TPA–TRDN[146] (Table 1), with a similar structure by extending the conjugation system of DPAR. This probe was extremely sensitive for detecting HSA (LOD = 0.34 μg mL^{-1}, 60-fold fluorescence response), and was also used to detect HSA in actual urine samples and recognize cancer cells. This indicated that the probe had potential for application in biomedical research related to microenvironments.

In 2024, Deng and his co-authors[147] created a TPA-based polarity sensitive NIR fluorescent probe, BTPA, for the detec-

tion of HSA. The probe had a typical D–π–A structure and exhibited the ICT effect. Photophysical analysis showed that as the solvent polarity increased, the maximum emission wavelength of BTPA shifted from 654 nm to 757 nm. In addition, when BTPA bound to HSA, the fluorescence intensity increased sharply by 50 times and displayed a large Stokes shift (~190 nm). BTPA had excellent selectivity and anti-interference ability for detecting HSA, and it has been successfully used for the detection of HSA in human urine samples, demonstrating a fast response (<30 s) and low LOD (0.12 μM).

At present, most of the fluorescent probes used for HSA detection exhibit "off–on" fluorescent responses, and few ratiometric fluorescent probes could achieve timely detection of HSA with the assistance of portable devices such as smartphones. Accordingly, Chen *et al.*[148] used a flavonoid probe (DMAF) with the D–A structure as a control to adjust the TICT and ICT effects of the molecular skeleton by changing the receptor structure. Combined with photophysical testing, they successfully screened out a fluorescent probe, STF, which showed high sensitivity to polarity changes. Binding to HSA placed the probe in a lower polarity environment, resulting in a ratiometric fluorescence response to HSA and a colorimetric change from blue to green. The probe had high sensitivity (LOD = 54 nM), excellent selectivity, and a fast response (<10 s) for detecting HSA. More interestingly, with the help of integrated detection equipment and a smartphone, the probe could achieve the timely detection of HSA in serum samples, and the detection results for HSA could also be recorded and analyzed through paper or 3D printed devices. This work not only provided a promising analytical tool for the timely detection of HSA, but also provided an effective strategy for regulating the fluorescence response mode of D–A probes.

Xu's research group[149] designed a fluorescent probe, C1, based on ESIPT for the specific detection of HSA. C1 exhibited dual emissions at 466 nm and 600 nm in water, which were attributed to the open-loop and closed-loop isomers of C1, respectively. As the polarity of the medium decreased, the fluorescence intensity of C1 increased at 466 nm, while the opposite change was observed at 600 nm, indicating the polarity dependence of the fluorescence emission of C1. When probe C1 bound to HSA, the low polarity environment inside the hydrophobic cavity of HSA promoted the transformation of C1 from an open-loop to a closed-loop isomer, resulting in a significant enhancement of the fluorescence at 446 nm; the interaction with BSA was manifested by a fluorescence enhancement at 512 nm. After C1 bound with HSA and BSA, the fluorescence color of C1 was also different, indicating that C1 could distinguish between these two proteins through differences in fluorescence signals. More impressively, C1 could measure HSA in human blood based on the change in fluorescence color on the test strip. This probe provided a new strategy for the development of more specific HSA fluorescent probes.

Polarity and others

Carboxyesterase (CE) belongs to the α/β-hydrolase folding family and is commonly found in various living systems.[150] CE plays a crucial role in catalyzing the hydrolysis of endogenous esters and foreign compounds.[151,152] In addition, CE has a close connection with metabolic diseases and is considered to be a unique indicator for hepatocellular carcinoma (HCC).[4,153] Recently, Rong *et al.*[154] reported the use of the fluorescent probe LD–TCE (Fig. 12(a)) for monitoring CE and LD polarity in liver cancer cells. The probe used carbamate as the recognition receptor for CE and had a favorable linear relationship with CE between 0 and 6 U mL^{-1}. Due to the presence of the polarity sensitive unit TPA, the probe emitted significantly enhanced fluorescence in low polarity media. When the probe entered liver cancer cells, it first interacted with over-expressed CE and released weak green fluorescence. Subsequently, it was further influenced by internal low polarity LDs, and the green fluorescence was further enhanced. Based on this cascade reaction, specific imaging of liver cancer cells was successfully achieved. In addition, the probe also achieved the localization of liver cancer in living mice. This probe not only provided a potential tool for the diagnosis of early liver cancer, but offered a new idea for the sequential detection of multiple analytes.

Based on OR logic gates, Zhu's group[155] developed a NIR fluorescent probe, VPCPP (Fig. 12(b)), that could track viscosity, polarity, and CE in the blue and red channels, respectively. This probe was successfully used for the identification of cancer cells. Owing to the elevated degree of CE in liver cell lines, the probe could also visualize liver cell lines in the blue channel. More interestingly, based on high-content analysis and VPCPP, a high-throughput screening (HTS) platform was first constructed to investigate the effect of anticancer drugs on the three parameters. Besides, the elevation of the CE level induced by aristolochic acid (AA) and the changes in these three parameters in the inflammatory model were successfully confirmed by intracellular imaging of dual emission channels. Finally, the probe also achieved the dual channel *ex vivo* imaging of tumors, liver, and kidneys, as well as single emission fluorescence imaging of tumors *in vivo*. This probe has potential for applications in clinical research and medical diagnosis.

Nitroreductase (NTR) is closely related to the level of hypoxia and regarded as a symbolic hallmark for tumors.[156,157] In the same year, the research group designed a fluorescent probe, VPHPP[158] (Fig. 12(c)), based on a structure similar to that of VPCPP, which could simultaneously detect polarity, viscosity, and NTR in dual channels. The *p*-nitrobenzene unit in the VPHPP structure relied on the PET mechanism to act as a recognition group for NTR. When NTR was present, the nitro group was reduced, resulting in the formation of an amino group, and the fluorescence was emitted at 540 nm owing to the end of the PET process. When VPHPP was in a low polarity, high viscosity environment, it emitted bright fluorescence in the NIR channel (747–810 nm). Using VPHPP, changes in viscosity, polarity, and NTR in live cells were observed simultaneously under hypoxic conditions. In MCF-7 cells, based on dual channel imaging of VPHPP, it was successfully observed that dicoumarin-induced down-regu-

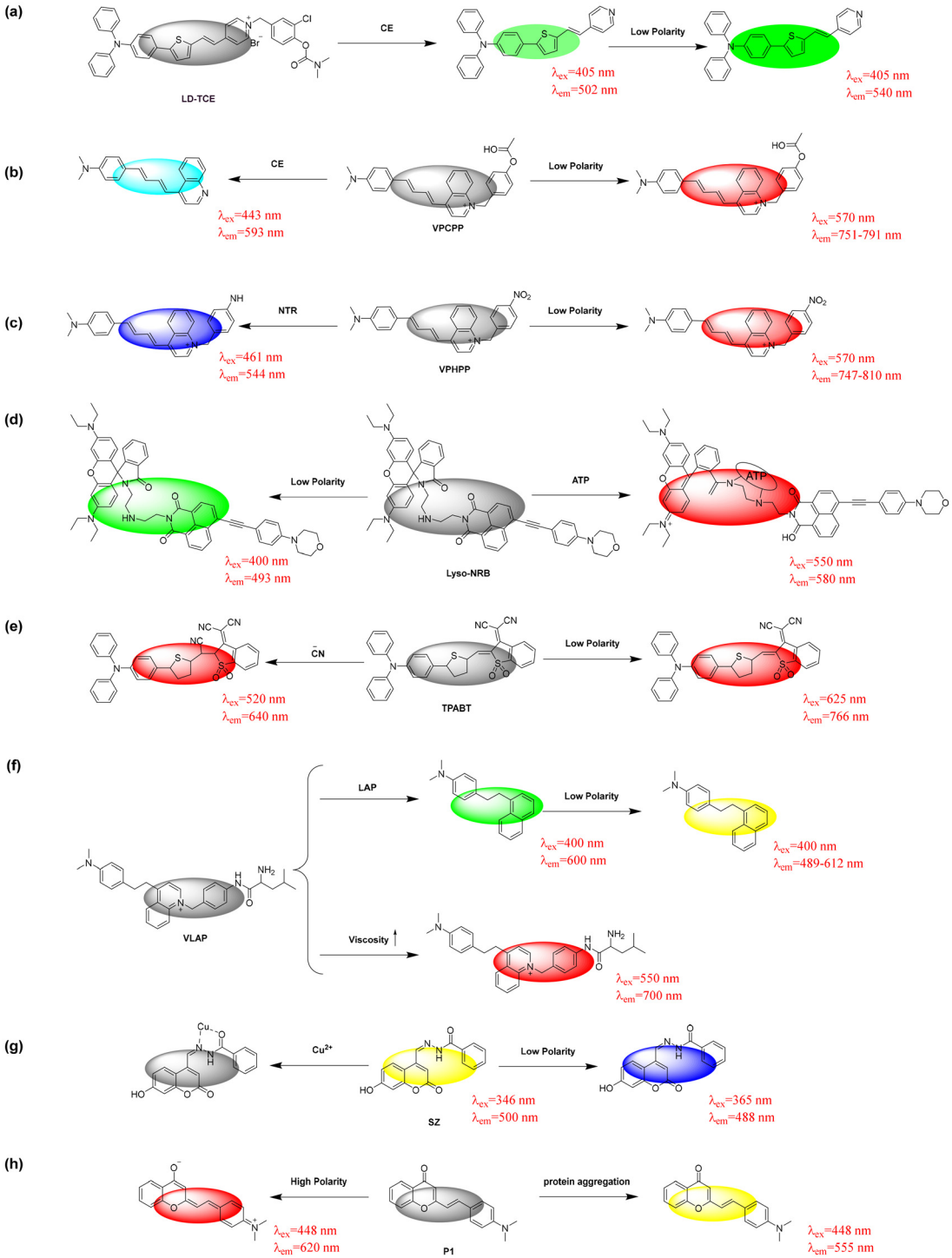

Fig. 12 Fluorescent probes for detecting polarity and other analytes.

lation of NTR was accompanied by a decrease in polarity and increase in viscosity. In addition, this multifunctional fluorescent probe enabled the diagnosis of cancer at the cellular level and *in vivo* through two channels. VPHPP's long retention time (20 h) and red light emission in tumors might become a potential contrast agent for imaging-guided surgical treatment.

Autophagy is an endocellular degradation pathway that relies on the lysosome and is crucial for preserving cellular homeostasis.[159–162] Changes in lysosome polarity and ATP are important markers of this process.[163] For this purpose, Jiang *et al.*[164] designed a bifunctional probe, Lyso–NRB, as depicted in Fig. 12(d), that could monitor lysosome polarity and ATP. The morpholine group in the Lyso–NRB structure served as the

targeting unit for the lysosome. The probe had a typical ICT effect. When it was in a low-polarity environment, Lyso–NRB emitted bright green fluorescence. In addition, after ATP was added, the spiro ring of rhodamine in Lyso–NRB was opened, releasing strong red fluorescence. The probe had excellent sensitivity and specificity for detecting polarity and ATP, and the LOD for ATP was as low as 33.3 μM. Using H_2O_2 or starvation to induce cellular autophagy, changes in lysosome polarity and ATP during this process were successfully observed through fluorescence imaging. More importantly, the probe was also successfully used to visualize the polarity and ATP fluctuations caused by oxidative stress-induced autophagy in zebrafish. This probe provided a favorable tool for further research on the autophagy process.

It is well known that cyanide (CN^-) is an extremely toxic substance to humans.[165] A dual functional fluorescent probe (TPABT) (Fig. 12(e)) for the simultaneous detection of polarity and CN^- was designed by Peng *et al.*[166] The probe also used TPA as a fluorophore and polarity sensitive unit. With the solvent polarity decreasing from water to 1,4-dioxane, the fluorescence emission of TPABT increased by 71-fold and shifted to the NIR region (766 nm). Based on this, the probe achieved the recognition of cancer cells and visualization of polarity changes in 4TI cells. Meanwhile, the presence of a vinyl bond enabled TPABT to detect CN^- under far-red light (640 nm) with a LOD as low as 22 nM. In addition, the probe was successfully used for the detection of CN^- in actual water samples and live cells.

Leucine aminopeptidase (LAP) is an enzyme that catalyzes the hydrolysis of leucine residues.[167,168] Abnormal expression or the catalytic function of LAP is associated with various diseases, such as significantly elevated levels in inflammation and cancer cells.[169,170] Li *et al.*[171] proposed a probe, VLAP (Fig. 12(f)), for the multi-color imaging of viscosity, polarity, and LAP simultaneously. VLAP had a typical D–π–A system, and the presence of a quinoline quaternary ammonium salt enabled it to target mitochondria. When VLAP was in a high viscosity environment, TICT was inhibited and produced a bright fluorescence signal at 700 nm. The leucine unit specifically combined with LAP, generating VLAPF. As a result, the ICT effect was weakened, and the fluorescence spectrum shifted to 600 nm.

Abnormal copper contents in organisms can cause diseases such as cirrhosis and Wilson's disease.[172,173] Excess copper in the environment poses a notable problem to the stability of an ecosystem.[174] Therefore, the development of an effective detection method for Cu^{2+} is urgently needed. Deng *et al.*[175] synthesized a coumarin-based fluorescent probe (SZ) (Fig. 12(g)) for the detection of Cu^{2+} and water in organic solvents. SZ was sensitive to polarity and displayed solvent-dependent fluorescence emission, and it had a low LOD (0.0035% (v/v)) for detecting water in ethanol. SZ showed a fast response (30 s) and high sensitivity (LOD = 9.6×10^{-8} mol L^{-1}) for Cu^{2+}. Given the excellent spectral performance of SZ, it was further utilized for the determination of Cu^{2+} in soil and environmental water samples. In addition, SZ was also successfully used for the determination of alcohol contents in white wine and moisture contents in sugar and salt samples.

Wan and Zeng *et al.*[176] reported a crystallization-induced emission (CIE) fluorescent probe, P1 (Fig. 12(h)), for determining the polarity of protein aggregates. Due to the ICT and TICT effects within the molecule, the maximum fluorescence emission of P1 was influenced by polarity and viscosity. In a crystalline solid, the ordered π–π stacking inhibited its rotation, resulting in fluorescence activation. However, in non-crystalline precipitate, P1 showed no emission, indicating that it exhibited CIE. The polarity heterogeneity between different aggregated proteins was revealed through P1 and matched with the resistance to protein hydrolysis. In addition, by monitoring the polarity dynamics of different proteins during misfolding and aggregation using P1, the outcomes revealed that the decrease in polarity was primarily focused on the formation process of soluble aggregates, while insoluble aggregates remained almost unchanged. More importantly, P1 successfully quantified the polarity of target protein aggregates in cells, further revealing the polarity heterogeneity of protein aggregates.

Conclusions

In recent years, the rapid development of fluorescence technology and the need for the precise identification and therapy of illnesses have jointly promoted the exploration of fluorescent probes in the bioimaging of pathophysiological microenvironments. In this review, we summarized the design concept, spectral properties and the bioimaging applications of versatile fluorescent probes for the concurrent determination of polarity and analytes over the past five years. At present, the reported multifunctional probes can not only successfully achieve the visualization and monitoring of polarity and analytes within physiological processes, including autophagy, FPT, and oxidative stress, but be applied to a variety of pathological processes including neurodegenerative disorders, cancer, inflammatory conditions, and fatty liver, which provide important visual evidence for the exploration of related processes underlying physiological and pathological states. Despite the fact that significant progress has been achieved in the development of versatile fluorescent probes targeting polarity and analytes, several problems still remain to be resolved. In the first place, a large number of the fluorescent probes currently mentioned for detecting polarity still suffer from photobleaching and are influenced by other microenvironmental parameters within the cells, such as pH and viscosity. Secondly, probes modified with a single fluorophore are prone to interference through spectral overlap in the sensing of polarity and relevant analytes. Thirdly, currently developed versatile fluorescent probes are rarely used in the NIR-II region (1000–1700 nm), which has significant advantages for deep tissue or biological imaging *in vivo*. To address these challenges in current multifunctional fluorescent probes, we believe that the design of probe structures can be approached from the following

aspects: (1) two or more fluorescent groups should be selected, as far as possible, within a single probe; this type of probe has the advantages of high quantum yield, adjustable targeting, and greatly reduced spectral overlap; (2) by enhancing the rigidity of fluorescent groups, photoisomerization can be reduced and the photobleaching rate can be lowered; (3) fluorophores that emit red light, or extending the conjugated system of the probe structure, enable the probe to respond to analytes in the long wavelength region; (4) integration with multimodal imaging (such as SRM, PAI, TPE, FLIM), as needed, yields richer and more accurate information.

In summary, the use of these multifunctional fluorescent probes for detecting polarity and analytes is expected to yield outstanding results for the investigation of various physiological and pathological mechanisms. This will provide insights into biological advances in drug discovery and diagnostic imaging.

Data availability

No primary research results, software or code have been included and no new data were generated or analysed as part of this review.

Conflicts of interest

The authors declare that they have no known competing financial interests or personal relationships that could have appeared to influence the work reported in this paper.

Acknowledgements

This work was financially supported by Shanxi University's Training Program of Innovation for Undergraduates (No. X202310108202).

References

1 X. Michalet, S. Weiss and M. Jäger, Single-Molecule Fluorescence Studies of Protein Folding and Conformational Dynamics, *Chem. Rev.*, 2006, **106**, 1785–1813.
2 N. Jiang, J. Fan, F. Xu, X. Peng, H. Mu, J. Wang and X. Xiong, Ratiometric Fluorescence Imaging of Cellular Polarity: Decrease in Mitochondrial Polarity in Cancer Cells, *Angew. Chem., Int. Ed.*, 2015, **54**, 2510–2514.
3 T. Tohmonda, A. Kamiya, A. Ishiguro, T. Iwaki, T. J. Fujimi, M. Hatayama, J. Aruga and J. R. True, Identification and Characterization of Novel Conserved Domains in Metazoan Zic Proteins, *Mol. Biol. Evol.*, 2018, **35**, 2205–2229.
4 S. Wang, W. X. Ren, J.-T. Hou, M. Won, J. An, X. Chen, J. Shu and J. S. Kim, Fluorescence imaging of pathophysiological microenvironments, *Chem. Soc. Rev.*, 2021, **50**, 8887–8902.
5 J. Zhao, S. Xue, R. Ji, B. Li and J. Li, Localized surface plasmon resonance for enhanced electrocatalysis, *Chem. Soc. Rev.*, 2021, **50**, 12070–12097.
6 M. W. Berns, T. Krasieva, C.-H. Sun, A. Dvornikov and P. M. Rentzepis, A polarity dependent fluorescence "switch" in live cells, *J. Photochem. Photobiol., B*, 2004, **75**, 51–56.
7 M. Lee and V. Vasioukhin, Cell polarity and cancer – cell and tissue polarity as a non-canonical tumor suppressor, *J. Cell Sci.*, 2008, **121**, 1141–1150.
8 Y.-D. Zhuang, P.-Y. Chiang, C.-W. Wang and K.-T. Tan, Environment-Sensitive Fluorescent Turn-On Probes Targeting Hydrophobic Ligand-Binding Domains for Selective Protein Detection, *Angew. Chem., Int. Ed.*, 2013, **52**, 8124–8128.
9 Z. Yang, J. Cao, Y. He, J. H. Yang, T. Kim, X. Peng and J. S. Kim, Macro-/micro-environment-sensitive chemosensing and biological imaging, *Chem. Soc. Rev.*, 2014, **43**, 4563–4601.
10 X. Li, X. Li and H. Ma, A near-infrared fluorescent probe reveals decreased mitochondrial polarity during mitophagy, *Chem. Sci.*, 2020, **11**, 1617–1622.
11 H. Li, H. Kim, F. Xu, J. Han, Q. Yao, J. Wang, K. Pu, X. Peng and J. Yoon, Correction: Activity-based NIR fluorescent probes based on the versatile hemicyanine scaffold: design strategy, biomedical applications, and outlook, *Chem. Soc. Rev.*, 2022, **51**, 1836–1836.
12 C. R. Santos and A. Schulze, Lipid metabolism in cancer, *FEBS J.*, 2012, **279**, 2610–2623.
13 F. Baenke, B. Peck, H. Miess and A. Schulze, Hooked on fat: the role of lipid synthesis in cancer metabolism and tumour development, *Dis. Models Mech.*, 2013, **6**, 1353–1363.
14 J. Yin, M. Peng, Y. Ma, R. Guo and W. Lin, Rational design of a lipid-droplet-polarity based fluorescent probe for potential cancer diagnosis, *Chem. Commun.*, 2018, **54**, 12093–12096.
15 J. Yin, M. Peng and W. Lin, Two-photon fluorescence imaging of lipid drops polarity toward cancer diagnosis in living cells and tissue, *Sens. Actuators, B*, 2019, **288**, 251–258.
16 S. Samanta, M. Huang, F. Lin, P. Das, B. Chen, W. Yan, J.-J. Chen, K. Ji, L. Liu, J. Qu and Z. Yang, Solo Smart Fluorogenic Probe for Potential Cancer Diagnosis and Tracking in Vivo Tumorous Lymphatic Systems via Distinct Emission Signals, *Anal. Chem.*, 2020, **92**, 1541–1548.
17 C. Soto, Unfolding the role of protein misfolding in neurodegenerative diseases, *Nat. Rev. Neurosci.*, 2003, **4**, 49–60.
18 M. S. Hipp, P. Kasturi and F. U. Hartl, The proteostasis network and its decline in ageing, *Nat. Rev. Mol. Cell Biol.*, 2019, **20**, 421–435.
19 B. L. Drees, B. Sundin, E. Brazeau, J. P. Caviston, G.-C. Chen, W. Guo, K. G. Kozminski, M. W. Lau,

J. J. Moskow, A. Tong, L. R. Schenkman, A. McKenzie III, P. Brennwald, M. Longtine, E. Bi, C. Chan, P. Novick, C. Boone, J. R. Pringle, T. N. Davis, S. Fields and D. G. Drubin, A protein interaction map for cell polarity development, *J. Cell Biol.*, 2001, **154**, 549–576.

20 H. R. Pires and M. Boxem, Mapping the Polarity Interactome, *J. Mol. Biol.*, 2018, **430**, 3521–3544.

21 K. W. Kurgan, A. F. Kleman, C. A. Bingman, D. F. Kreitler, B. Weisblum, K. T. Forest and S. H. Gellman, Retention of Native Quaternary Structure in Racemic Melittin Crystals, *J. Am. Chem. Soc.*, 2019, **141**, 7704–7708.

22 D. I. Danylchuk, P.-H. Jouard and A. S. Klymchenko, Targeted Solvatochromic Fluorescent Probes for Imaging Lipid Order in Organelles under Oxidative and Mechanical Stress, *J. Am. Chem. Soc.*, 2021, **143**, 912–924.

23 N. Li, W. Qin, Y. Chen, K. Liu, S. Wang and F. Kong, Construction of a robust polarity sensitive platform and its application for tracking of lipid droplets decrease under oxidative stress in live cells, *Sens. Actuators, B*, 2021, **346**, 130491.

24 Z. Zhan, R. Huang, L. Chai, H. Yang, Y. Dai, M. Chen, G. Gu and Y. Lv, Fluorescence lifetime imaging: A novel approach to simultaneous visualizing lipid droplets and endoplasmic reticulum polarity in live cells and fatty liver, *Sens. Actuators, B*, 2025, **422**, 136699.

25 Y. Yue, F. Huo, X. Li, Y. Wen, T. Yi, J. Salamanca, J. O. Escobedo, R. M. Strongin and C. Yin, pH-Dependent Fluorescent Probe That Can Be Tuned for Cysteine or Homocysteine, *Org. Lett.*, 2017, **19**, 82–85.

26 H.-H. Han, H. Tian, Y. Zang, A. C. Sedgwick, J. Li, J. L. Sessler, X.-P. He and T. D. James, Small-molecule fluorescence-based probes for interrogating major organ diseases, *Chem. Soc. Rev.*, 2021, **50**, 9391–9429.

27 X. Ren, L. Liao, Z. Yang, H. Li, X. Li, Y. Wang, Y. Ye and X. Song, Rational design of a bifunctional fluorescent probe for distinguishing Hcy/Cys from GSH with ideal properties, *Chin. Chem. Lett.*, 2021, **32**, 1061–1065.

28 J. Tang, X. Yang, F. Zhao, D. Zhang, S. Mo and Y. Ye, Visualizing peroxynitrite fluxes and protective effect of endogenous hydrogen sulfide during carbonyl stress in endothelial cell, *Sens. Actuators, B*, 2021, **330**, 129283.

29 S. Lee, J. Li, X. Zhou, J. Yin and J. Yoon, Recent progress on the development of glutathione (GSH) selective fluorescent and colorimetric probes, *Coord. Chem. Rev.*, 2018, **366**, 29–68.

30 R. Zhang, J. Yong, J. Yuan and Z. Ping Xu, Recent advances in the development of responsive probes for selective detection of cysteine, *Coord. Chem. Rev.*, 2020, **408**, 213182.

31 D.-J. Zheng, Y.-S. Yang and H.-L. Zhu, Recent progress in the development of small-molecule fluorescent probes for the detection of hydrogen peroxide, *TrAC, Trends Anal. Chem.*, 2019, **118**, 625–651.

32 J. Chan, S. C. Dodani and C. J. Chang, Reaction-based small-molecule fluorescent probes for chemoselective bioimaging, *Nat. Chem.*, 2012, **4**, 973–984.

33 A. T. Aron, K. M. Ramos-Torres, J. A. Cotruvo Jr. and C. J. Chang, Recognition- and Reactivity-Based Fluorescent Probes for Studying Transition Metal Signaling in Living Systems, *Acc. Chem. Res.*, 2015, **48**, 2434–2442.

34 J. Li, G. Zuo, X. Qi, W. Wei, X. Pan, T. Su, J. Zhang and W. Dong, Selective determination of Ag+ using Salecan derived nitrogen doped carbon dots as a fluorescent probe, *Mater. Sci. Eng., C*, 2017, **77**, 508–512.

35 Y. Yue, F. Huo, P. Ning, Y. Zhang, J. Chao, X. Meng and C. Yin, Dual-Site Fluorescent Probe for Visualizing the Metabolism of Cys in Living Cells, *J. Am. Chem. Soc.*, 2017, **139**, 3181–3185.

36 Y.-R. Zhang, Y. Liu, X. Feng and B.-X. Zhao, Recent progress in the development of fluorescent probes for the detection of hypochlorous acid, *Sens. Actuators, B*, 2017, **240**, 18–36.

37 A. C. Sedgwick, H.-H. Han, J. E. Gardiner, S. D. Bull, X.-P. He and T. D. James, The development of a novel AND logic based fluorescence probe for the detection of peroxynitrite and GSH, *Chem. Sci.*, 2018, **9**, 3672–3676.

38 S. Cheng, A. Li, X. Pan, H. Wang, C. Zhang, J. Li and X. Qi, A near-infrared fluorescent probe for highly specific and ultrasensitive detection of hypochlorite ions in living cells, *Anal. Bioanal. Chem.*, 2021, **413**, 4441–4450.

39 S. Ye, H. Zhang, J. Fei, C. H. Wolstenholme and X. Zhang, A General Strategy to Control Viscosity Sensitivity of Molecular Rotor-Based Fluorophores, *Angew. Chem., Int. Ed.*, 2021, **60**, 1339–1346.

40 R. Zhang, J. Zhao, G. Han, Z. Liu, C. Liu, C. Zhang, B. Liu, C. Jiang, R. Liu, T. Zhao, M.-Y. Han and Z. Zhang, Real-Time Discrimination and Versatile Profiling of Spontaneous Reactive Oxygen Species in Living Organisms with a Single Fluorescent Probe, *J. Am. Chem. Soc.*, 2016, **138**, 3769–3778.

41 H. Zhu, J. Fan, J. Du and X. Peng, Fluorescent Probes for Sensing and Imaging within Specific Cellular Organelles, *Acc. Chem. Res.*, 2016, **49**, 2115–2126.

42 W. Zhang, J. Liu, P. Li, X. Wang, S. Bi, J. Zhang, W. Zhang, H. Wang and B. Tang, In situ and real-time imaging of superoxide anion and peroxynitrite elucidating arginase 1 nitration aggravating hepatic ischemia-reperfusion injury, *Biomaterials*, 2019, **225**, 119499.

43 X. Yang, D. Zhang, Y. Ye and Y. Zhao, Recent advances in multifunctional fluorescent probes for viscosity and analytes, *Coord. Chem. Rev.*, 2022, **453**, 214336.

44 B. Uttekar, R. K. Verma, D. Tomer and R. Rikhy, Mitochondrial morphology dynamics and ROS regulate apical polarity and differentiation in Drosophila follicle cells, *Development*, 2024, **151**, dev201732.

45 Z. Kang, Y. Zhou, W. Wang, S. Wang, S. Wen, H. Yu, X. Liu, J. Wang and M.-S. Yuan, Dual-response chemosensor for monitoring changes of polarity and ·OH in ferroptosis of cell and zebrafish, *Sens. Actuators, B*, 2025, **426**, 137121.

46 J. L. Kolanowski, F. Liu and E. J. New, Fluorescent probes for the simultaneous detection of multiple analytes in biology, *Chem. Soc. Rev.*, 2018, **47**, 195–208.

47 K. Zhou, Y. Yang, T. Zhou, M. Jin and C. Yin, Design strategy of multifunctional and high efficient hydrogen sulfide NIR fluorescent probe and its application in vivo, *Dyes Pigm.*, 2021, **185**, 108901.
48 Y. Liu, L. Teng, C. Xu, H.-W. Liu, S. Xu, H. Guo, L. Yuan and X.-B. Zhang, A "Double-Locked" and enzyme-activated molecular probe for accurate bioimaging and hepatopathy differentiation, *Chem. Sci.*, 2019, **10**, 10931–10936.
49 W. Zhang, F. Huo, F. Cheng and C. Yin, Employing an ICT-FRET Integration Platform for the Real-Time Tracking of SO2 Metabolism in Cancer Cells and Tumor Models, *J. Am. Chem. Soc.*, 2020, **142**, 6324–6331.
50 X. Tian, L. C. Murfin, L. Wu, S. E. Lewis and T. D. James, Fluorescent small organic probes for biosensing, *Chem. Sci.*, 2021, **12**, 3406–3426.
51 J. Xu, Q. Tian, Q. Chu, Y. Zhang, M. Zou, H. Zhao, Y. Liu and W. Chu, Design and synthesis of phenothiazine-based D–A molecules with ICT characteristics as efficient fluorescent probes for detecting hypochlorite in water, *Spectrochim. Acta, Part A*, 2025, **328**, 125491.
52 C. Wang, W. Chi, Q. Qiao, D. Tan, Z. Xu and X. Liu, Twisted intramolecular charge transfer (TICT) and twists beyond TICT: from mechanisms to rational designs of bright and sensitive fluorophores, *Chem. Soc. Rev.*, 2021, **50**, 12656–12678.
53 W. Sun, M. Li, J. Fan and X. Peng, Activity-Based Sensing and Theranostic Probes Based on Photoinduced Electron Transfer, *Acc. Chem. Res.*, 2019, **52**, 2818–2831.
54 D. Zhang, R. Duan, X. Zhou, Z. Ma, J. Shi, H. Chen, J. Guo, M. Li, T. Wang and X. Wu, A naphthimide based fluorescent probe for the detection of thiophenols and its application in actual water and food, *J. Mol. Struct.*, 2025, **1322**, 140473.
55 Y. Li, D. Dahal, C. S. Abeywickrama and Y. Pang, Progress in Tuning Emission of the Excited-State Intramolecular Proton Transfer (ESIPT)-Based Fluorescent Probes, *ACS Omega*, 2021, **6**, 6547–6553.
56 C. Lu, J. Xu, Z. Song and Z. Dai, Advancements in ESIPT probe research over the past three years based on different fluorophores, *Dyes Pigm.*, 2024, **224**, 111994.
57 H. B. Xiao, P. Li and B. Tang, Recent progresses in fluorescent probes for detection of polarity, *Coord. Chem. Rev.*, 2021, **427**, 213582.
58 V. Nguyen and H. D. Li, Recent Development of Lysosome-Targeted Organic Fluorescent Probes for Reactive Oxygen Species, *Molecules*, 2023, **28**, 6650.
59 X. T. Jing, F. B. Yu and L. X. Chen, Fluorescent Probes for Reactive Nitrogen Species, *Prog. Chem.*, 2014, **26**, 866–878.
60 P. Huang, Y. K. Yue, C. X. Yin and F. J. Huo, Design of Dual-responsive ROS/RSS Fluorescent Probes and Their Application in Bioimaging, *Chem. – Asian J.*, 2022, **17**, e202200907.
61 J. Y. Yang, Z. Z. Zhao, S. Y. Jiang, L. Y. Zhang, K. Zhao, Z. T. Li and D. Ma, pH-sensing supramolecular fluorescent probes discovered by library screening, *Talanta*, 2023, **263**, 124716.
62 H. B. Xiao, P. Li and B. Tang, Small Molecular Fluorescent Probes for Imaging of Viscosity in Living Biosystems, *Chem. – Eur. J.*, 2021, **27**, 6880–6898.
63 T. Y. Z. Lü, K. N. Zhu and B. Liu, Recent Advances of Organic Fluorescent Probes for Detection of Human Serum Albumin, *Chin. J. Org. Chem.*, 2019, **39**, 2786–2795.
64 R. N. da Silva, C. C. Costa, M. J. G. Santos, M. Q. Alves, S. S. Braga, S. I. Vieira, J. Rocha, A. M. S. Silva and S. Guieu, Fluorescent Light-up Probe for the Detection of Protein Aggregates, *Chem. – Asian J.*, 2019, **14**, 859–863.
65 J. Q. Leng, X. Y. Lan, W. S. Jiang, J. Y. Xiao, T. X. Liu and Z. B. Liu, Molecular Fluorescent Probe for Detection of Metal Ions, *Spectrosc. Spectral Anal.*, 2023, **43**, 1993–2011.
66 X. Chen, X. Tian, I. Shin and J. Yoon, Fluorescent and luminescent probes for detection of reactive oxygen and nitrogen species, *Chem. Soc. Rev.*, 2011, **40**, 4783–4804.
67 J. F. Woolley, J. Stanicka and T. G. Cotter, Recent advances in reactive oxygen species measurement in biological systems, *Trends Biochem. Sci.*, 2013, **38**, 556–565.
68 X. Yang, J. Liu, P. Xie, X. Han, D. Zhang, Y. Ye and Y. Zhao, Visualization of biothiols and HClO in cancer therapy via a multi-responsive fluorescent probe, *Sens. Actuators, B*, 2021, **347**, 130620.
69 H. Mu, Y. Zhang, P. Zheng and M. Zhang, Ultrafast fluorescence probe to H_2O_2 vapor based on organic-inorganic hybrid silica nanoparticles, *Talanta*, 2022, **237**, 122914.
70 M. Li, W. Fang, B. Wang, Y. Du, Y. Hou, L. Chen, S. Cui, Y. Li and X. Yan, A novel dual-site ICT/AIE fluorescent probe for detecting hypochlorite and polarity in living cells, *New J. Chem.*, 2021, **45**, 21406–21414.
71 X. Wang, Z. Gou, J.-J. Lv and Y. Zuo, A novel coumarin-TPA based fluorescent probe for turn-on hypochlorite detection and lipid-droplet-polarity bioimaging in cancer cells, *Spectrochim. Acta, Part A*, 2022, **279**, 121481.
72 A. Weiland, Y. Wang, W. Wu, X. Lan, X. Han, Q. Li and J. Wang, Ferroptosis and Its Role in Diverse Brain Diseases, *Mol. Neurobiol.*, 2019, **56**, 4880–4893.
73 D. Wu and L. Chen, Ferroptosis: a novel cell death form will be a promising therapy target for diseases, *Acta Biochim. Biophys. Sin.*, 2015, **47**, 857–859.
74 K. Wang, X. Z. Chen, Y. H. Wang, X. L. Cheng, Y. Zhao, L. Y. Zhou and K. Wang, Emerging roles of ferroptosis in cardiovascular diseases, *Cell Death Discovery*, 2022, **8**, 394.
75 B. R. Stockwell, Ferroptosis turns 10: Emerging mechanisms, physiological functions, and therapeutic applications, *Cell*, 2022, **185**, 2401–2421.
76 X. Xu, J. Liu, D. Zhang and Y. Ye, A novel NIR LDs-targeted fluorescent probe to image HClO and polarity during ferroptosis, *Dyes Pigm.*, 2023, **219**, 111552.
77 Q. He, T. Guo, M. Lan, S. Zhao, S. Han, C. Yao and X. Song, Dual-ratiometric fluorescent probes for monitoring ClO- and polarity dynamics in ferroptosis, *Sens. Actuators, B*, 2024, **415**, 136030.
78 T. Yang, Y. Fang, Q. Zhang, F. Wang, X. Xu and C. Li, Lipid droplets-targeting multifunctional fluorescent probe

and its application in ferroptosis and bioimaging, *Sens. Actuators, B*, 2024, **417**, 136138.

79 M. Li, B. Wang, J. Liu, Z. Zhang, L. Chen, Y. Li and X. Yan, Lipid Droplet-Specific Dual-Response Fluorescent Probe for the Detection of Polarity and H_2O_2 and Its Application in Living Cells, *Anal. Chem.*, 2022, **94**, 9732–9739.

80 X. Tian, J. Cheng, L. Yang, Z. Li and M. Yu, A NIR Dual-Channel Fluorescent Probe for Fluctuations of Intracellular Polarity and H_2O_2 and Its Applications for the Visualization of Inflammation and Ferroptosis, *Chem. Biomed. Imaging*, 2024, **2**, 518–525.

81 J. Liu, Y.-Q. Sun, Y. Huo, H. Zhang, L. Wang, P. Zhang, D. Song, Y. Shi and W. Guo, Simultaneous Fluorescence Sensing of Cys and GSH from Different Emission Channels, *J. Am. Chem. Soc.*, 2014, **136**, 574–577.

82 Z. Guo, S. Nam, S. Park and J. Yoon, A highly selective ratiometric near-infrared fluorescent cyanine sensor for cysteine with remarkable shift and its application in bioimaging, *Chem. Sci.*, 2012, **3**, 2760–2765.

83 Y. Liu, Y. Yu, Q. Zhao, C. Tang, H. Zhang, Y. Qin, X. Feng and J. Zhang, Fluorescent probes based on nucleophilic aromatic substitution reactions for reactive sulfur and selenium species: Recent progress, applications, and design strategies, *Coord. Chem. Rev.*, 2021, **427**, 213601.

84 Q. Zan, L. Fan, L. Ma, Q. Yang, K. Zhao, Y. Huang, C. Dong and S. Shuang, Dual-channel fluorescent probe for simultaneously detecting H_2S and viscosity/polarity and its application in non-alcoholic fatty liver, tumor tissue, and food spoilage, *Sens. Actuators, B*, 2023, **397**, 134596.

85 P. Xie, J. Liu, X. Yang, W. Zhu and Y. Ye, A bifunctional fluorescent probe for imaging lipid droplets polarity/SO2 during ferroptosis, *Sens. Actuators, B*, 2022, **365**, 131937.

86 S. Mu, T. Han, X. Zhang, J. Liu, H. Sun, J. Zhang, X. Liu and H. Zhang, Exploring the Role of Mitochondrial Hydrogen Sulfide in Maintaining Polarity and mtDNA Integrity with a Multichannel Fluorescent Probe, *Anal. Chem.*, 2023, **95**, 18460–18469.

87 L. Ma, Q. Zan, B. Zhang, W. Zhang, C. Jia and L. Fan, A multi-functional fluorescent probe for visualization of H_2S and viscosity/polarity and its application in cancer imaging, *Anal. Bioanal. Chem.*, 2024, **416**, 1375–1387.

88 S. Zhang, H. Zheng, L. Yang, Z. Li and M. Yu, NIR Mitochondrial Fluorescent Probe for Visualizing SO2/Polarity in Drug Induced Inflammatory Mice, *Anal. Chem.*, 2023, **95**, 5377–5383.

89 S. Wang, H. Zheng, L. Ma, L. Yang, Q. Song, M. Yu and Z. Li, Observation of diagnostic and therapeutic processes of inflammation and ferroptosis by a three-channel fluorescent probe, *Sens. Actuators, B*, 2024, **417**, 136113.

90 Y. Zhang, L. Tang, G. Yang, H. Xin, Y. Huang, K. Li, J. Liu, J. Pang and D. Cao, Coumarin-aurone based fluorescence probes for cysteine sensitive *in situ* identification in living cells, *Colloids Surf., B*, 2024, **244**, 114173.

91 L. Xiao, X. Sun, Z. Li, Y. Zhang, P. Zhang, Y. He, B. Guo, F. Yang and W. Shu, Recent progress in rational design of peroxynitrite fluorescent probes and bioapplication, *Dyes Pigm.*, 2023, **216**, 111385.

92 Y. Zhou, X. Kuang, X. Yang, J. Li, X. Wei, W. J. Jang, S.-S. Zhang, M. Yan and J. Yoon, Recent progress in small-molecule fluorescent probes for the detection of superoxide anion, nitric oxide, and peroxynitrite anion in biological systems, *Chem. Sci.*, 2024, **15**, 19669–19697.

93 L. Li, C. Wang, J. Hu and W.-H. Chen, Recent progress in organelle-targeting fluorescent probes for the detection of peroxynitrite, *Chem. Commun.*, 2024, **60**, 13629–13640.

94 D. Liu, G. Fang, Y. Wang, C. Meng, Z. Liu, Q. Chen and X. Shao, Facile construction of dual-response super-resolution probes for tracking organelles dynamics, *Exploration*, 2024, **4**, 20230145.

95 Y. Huang, M. Li, Q. Zan, R. Wang, S. Shuang and C. Dong, Mitochondria-Targeting Multifunctional Fluorescent Probe toward Polarity, Viscosity, and ONOO– and Cell Imaging, *Anal. Chem.*, 2023, **95**, 10155–10162.

96 L. Fan, Q. Yang, Q. Zan, K. Zhao, W. Lu, X. Wang, Y. Wang, S. Shuang and C. Dong, Multifunctional Fluorescent Probe for Simultaneous Detection of ONOO–, Viscosity, and Polarity and Its Application in Ferroptosis and Cancer Models, *Anal. Chem.*, 2023, **95**, 5780–5787.

97 Y.-Y. Li, J.-L. Hu, J.-R. Wu, Y.-R. Wang, A.-H. Zhang, Y.-W. Tan, Y.-J. Shang, T. Liang, M. Li, Y.-L. Meng and Y.-F. Kang, Multifunctional fluorescence probe for simultaneous detection of viscosity, polarity, and ONOO– and its bioimaging in vitro and vivo, *Biosens. Bioelectron.*, 2024, **254**, 116233.

98 D. Wencel, T. Abel and C. McDonagh, Optical Chemical pH Sensors, *Anal. Chem.*, 2014, **86**, 15–29.

99 L. Manjakkal, D. Szwagierczak and R. Dahiya, Metal oxides based electrochemical pH sensors: Current progress and future perspectives, *Prog. Mater. Sci.*, 2020, **109**, 100635.

100 Y. Liu, W. Yan, J. Li, Y. Wang, G. Zhang, L. Shi, C. Zhang, S. Shuang and C. Dong, Polarity, pH and HClO triple-response fluorescent probe and its application in inflammation models, *J. Mol. Liq.*, 2025, **422**, 126953.

101 L. Chao, Q. Zhang, L. Ga and J. Ai, Design, synthesis and application of polarity- and pH-sensitive dual-responsive small molecule fluorescent probe for early cancer diagnosis, *Microchem. J.*, 2024, **205**, 111250.

102 M. Sun and H. Y. Zhang, Par3 and aPKC regulate BACE1 endosome-to-TGN trafficking through PACS1, *Neurobiol. Aging*, 2017, **60**, 129–140.

103 R. Mallesh, J. Khan, K. Pradhan, R. Roy, N. R. Jana, P. Jaisankar and S. Ghosh, Design and Development of Benzothiazole-Based Fluorescent Probes for Selective Detection of Aβ Aggregates in Alzheimer's Disease, *ACS Chem. Neurosci.*, 2022, **13**, 2503–2516.

104 Z. Liang, Y. Sun, R. Duan, R. Yang, L. Qu, K. Zhang and Z. Li, Low Polarity-Triggered Basic Hydrolysis of Coumarin as an AND Logic Gate for Broad-Spectrum Cancer Diagnosis, *Anal. Chem.*, 2021, **93**, 12434–12440.

105 D. Thomas, V. Rubio, V. Iragavarapu, E. Guzman, O. B. Pelletier, S. Alamgir, Q. Zhang and M. J. Stawikowski,

Solvatochromic and pH-Sensitive Fluorescent Membrane Probes for Imaging of Live Cells, *ACS Chem. Neurosci.*, 2021, **12**, 719–734.

106 F. A. M. Al-Zahrani, Synthesis, Dynamics of Solvatochromism and pH-sensory of Novel Push-π-pull Phenothiazine-quinoline Fluorophore Toward Turn-on Fluorescent and Colorimetric Test Strips, *Fibers Polym.*, 2022, **23**, 1182–1189.

107 B. Razavi, H. Roghani-Mamaqani and M. Salami-Kalajahi, Rewritable acidochromic papers based on oxazolidine for anticounterfeiting and photosensing of polarity and pH of aqueous media, *Sci. Rep.*, 2022, **12**, 9412.

108 K.-I. Hong, K. H. Chu and W.-D. Jang, Thiophene-conjugated benzothiazole derivatives as versatile skeletons for staining subcellular organelles in living cells, *Dyes Pigm.*, 2023, **220**, 111753.

109 S. Ghosh, B. Zhao, J. Bie and J. Song, Macrophage cholesteryl ester mobilization and atherosclerosis, *Vasc. Pharmacol.*, 2010, **52**, 1–10.

110 S. K. Singh, M. V. Suresh, B. Voleti and A. Agrawal, The connection between C-reactive protein and atherosclerosis, *Ann. Med.*, 2008, **40**, 110–120.

111 Z.-L. Li, G.-M. Han, K. Wang, J.-A. Lyu, Z.-W. Li, B.-C. Zhu, L.-N. Zhu and D.-M. Kong, Multiparameter Assessment of Foam Cell Formation Progression Using a Dual-Color Switchable Fluorescence Probe, *Anal. Chem.*, 2024, **96**, 6968–6977.

112 M. Ren, Q. Xu, S. Wang, L. Liu and F. Kong, A biotin-guided fluorescent probe for dual-mode imaging of viscosity in cancerous cells and tumor tissues, *Chem. Commun.*, 2020, **56**, 13351–13354.

113 Y. Zhou, P. Li, X. Wang, C. Wu, N. Fan, X. Liu, L. Wu, W. Zhang, W. Zhang, Z. Liu and B. Tang, In situ visualization of peroxisomal viscosity in the liver of mice with non-alcoholic fatty liver disease by near-infrared fluorescence and photoacoustic imaging, *Chem. Sci.*, 2020, **11**, 12149–12156.

114 S. J. Singer and G. L. Nicolson, The Fluid Mosaic Model of the Structure of Cell Membranes, *Science*, 1972, **175**, 720–731.

115 M. J. Stutts, C. M. Canessa, J. C. Olsen, M. Hamrick, J. A. Cohn, B. C. Rossier and R. C. Boucher, CFTR as a cAMP-Dependent Regulator of Sodium Channels, *Science*, 1995, **269**, 847–850.

116 J. Cui, Y. Yao, C. Chen, R. Huang, W. Zhang and J. Qian, Mitochondria-targeted ratiometric fluorescent probes for micropolarity and microviscosity and their applications, *Chin. Chem. Lett.*, 2019, **30**, 1071–1074.

117 S. Martin and R. G. Parton, Lipid droplets: a unified view of a dynamic organelle, *Nat. Rev. Mol. Cell Biol.*, 2006, **7**, 373–378.

118 S.-O. Olofsson, P. Boström, L. Andersson, M. Rutberg, J. Perman and J. Borén, Lipid droplets as dynamic organelles connecting storage and efflux of lipids, *Biochim. Biophys. Acta, Mol. Cell Biol. Lipids*, 2009, **1791**, 448–458.

119 T. C. Walther and R. V. Farese, Lipid Droplets and Cellular Lipid Metabolism, *Annu. Rev. Biochem.*, 2012, **81**, 687–714.

120 C. Han, Z.-H. Zhang, L. Wang, X.-Q. Chen, J. Qu, K. Liu and J.-Y. Wang, Two reasonably designed polarity-viscosity sensitive fluorescent probes with large Stokes shift for lighting up lipid droplets in cells, *J. Photochem. Photobiol., A*, 2022, **425**, 113656.

121 M.-H. Wang, W.-L. Cui, Y.-H. Yang and J.-Y. Wang, Viscosity-Sensitive Solvatochromic Fluorescent Probes for Lipid Droplets Staining, *Biosensors*, 2022, **12**, 851.

122 C. Duangkamol, P. Muangsopa, S. Rattanopas, P. Wongsuwan, T. Khrootkaew, P. Chueakwon, N. Niamnont, K. Chansaenpak and A. Kamkaew, Polarity and viscosity-sensitive fluorescence probes for lipid droplet imaging in cancer cells, *Dyes Pigm.*, 2023, **216**, 111365.

123 S. Wang, X. Zhao, M. Liu, L. Yang, M. Yu and Z. Li, A dual-responsive crimson fluorescent probe for real-time diagnosis of alcoholic acute liver injury, *Biosens. Bioelectron.*, 2023, **239**, 115596.

124 Y. He, Y.-H. Yang, G.-Y. Chen, L. Li, L.-Q. Wang, L.-K. Li and J.-Y. Wang, A viscosity-sensitive fluorescent probe with a large Stokes shift for monitoring lipid droplets and its application in cell, tobacco leaf, and food detection, *New J. Chem.*, 2024, **48**, 12828–12833.

125 M. Chao, H. Zhang, Q. Hu, S. Ma, X. Cui, X. Zhu, J. Zhang and X. Yu, A novel π-bridge rationally designed polarity-viscosity-sensitive probe for lipid imaging, *Dyes Pigm.*, 2024, **225**, 112088.

126 C. Bian, M. Liu, J. Cheng, L. Yang, Z. Li and M. Yu, Dual-Functional Fluorescent Probe in the Diagnosis of Liver Injury and the Evaluation of Drug Therapy with Double Signal Amplification, *Chem. Biomed. Imaging*, 2024, **2**, 156–164.

127 E. Zhang, Q. Zhang, S. Wang, G. Zhang, A. Li, W. Lu and P. Ju, A dual-emission fluorescent probe with independent polarity and viscosity responses: The synthesis, spectroscopy and bio-imaging applications, *Spectrochim. Acta, Part A*, 2024, **323**, 124873.

128 Y. Zhu, X. Sun, Y. Yuan, X. Zhao, Z. Zhai, B. Song, W. Zhang, X. Zhu and X.-Q. Hao, Imidazo[1,2-α]pyridine-based polarity and viscosity-dependent fluorescent probes and application in selective detection of 2,6-dichloro-4-nitroaniline, *Dyes Pigm.*, 2024, **231**, 112425.

129 J. M. Long and D. M. Holtzman, Alzheimer Disease: An Update on Pathobiology and Treatment Strategies, *Cell*, 2019, **179**, 312–339.

130 E. Masliah, The Role of Synaptic Proteins in Alzheimer's Disease, *Ann. N. Y. Acad. Sci.*, 2000, **924**, 68–75.

131 H. Tsushima, M. Emanuele, A. Polenghi, A. Esposito, M. Vassalli, A. Barberis, F. Difato and E. Chieregatti, HDAC6 and RhoA are novel players in Abeta-driven disruption of neuronal polarity, *Nat. Commun.*, 2015, **6**, 7781.

132 J. An, P. Jangili, S. Lim, Y. K. Kim, P. Verwilst and J. S. Kim, Multichromatic fluorescence towards aberrant proteinaceous aggregates utilizing benzimidazole-based

ICT fluorophores, *J. Inclusion Phenom. Macrocyclic Chem.*, 2021, **101**, 205–215.
133 F. Fueyo-González, J. A. González-Vera, I. Alkorta, L. Infantes, M. L. Jimeno, P. Aranda, D. Acuña-Castroviejo, A. Ruiz-Arias, A. Orte and R. Herranz, Environment-Sensitive Probes for Illuminating Amyloid Aggregation In Vitro and in Zebrafish, *ACS Sens.*, 2020, **5**, 2792–2799.
134 L. Espinar-Barranco, J. M. Paredes, A. Orte, L. Crovetto and E. Garcia-Fernandez, A solvatofluorochromic dye as a fluorescent lifetime-based probe of β-amyloid aggregation, *Dyes Pigm.*, 2022, **202**, 110274.
135 J. Miao, M. Miao, Y. Jiang, M. Zhao, Q. Li, Y. Zhang, Y. An, K. Pu and Q. Miao, An Activatable NIR-II Fluorescent Reporter for In Vivo Imaging of Amyloid-β Plaques, *Angew. Chem., Int. Ed.*, 2023, **62**, e202216351.
136 S. E. Radford and C. M. Dobson, From Computer Simulations to Human Disease: Emerging Themes in Protein Folding, *Cell*, 1999, **97**, 291–298.
137 J. M. T. Hyttinen, M. Amadio, J. Viiri, A. Pascale, A. Salminen and K. Kaarniranta, Clearance of misfolded and aggregated proteins by aggrephagy and implications for aggregation diseases, *Ageing Res. Rev.*, 2014, **18**, 16–28.
138 S. Yang, X. Liu, S. Wang, J. Song, J. Wu, B. Shen, H. Jia, S. Guo, Y. Wang, Y. Yang, Y. Jiang, H. Yang and J. Chang, Chalcone derivatives as dual-sensitive fluorescent probe for protein aggregation investigation, *Sens. Actuators, B*, 2023, **395**, 134514.
139 G. Vázquez, A. Espargaró, A. B. Caballero, A. Di Pede-Mattatelli, M. A. Busquets, D. Nawrot, R. Sabaté, E. Nicolás, J. Juárez-Jiménez and P. Gamez, A versatile luminescent probe for sensing and monitoring amyloid proteins, *Dyes Pigm.*, 2024, **231**, 112348.
140 P. Sun, H.-C. Chen, W. Guo, Z. Zhang, S. Sun, N. Gao, Y.-H. Jing and B. Wang, A ratiometric fluorescent probe revealing the abnormality of acetylated tau by visualizing polarity in Alzheimer's disease, *J. Mater. Chem. B*, 2024, **12**, 5619–5627.
141 C.-E. Ha and N. V. Bhagavan, Novel insights into the pleiotropic effects of human serum albumin in health and disease, *Biochim. Biophys. Acta, Gen. Subj.*, 2013, **1830**, 5486–5493.
142 S. Samanta, S. Halder and G. Das, Twisted-Intramolecular-Charge-Transfer-Based Turn-On Fluorogenic Nanoprobe for Real-Time Detection of Serum Albumin in Physiological Conditions, *Anal. Chem.*, 2018, **90**, 7561–7568.
143 S. Halder, S. Samanta and G. Das, Exploring the potential of a urea derivative: an AIE-luminogen and its interaction with human serum albumin in aqueous medium, *Analyst*, 2019, **144**, 2696–2703.
144 N. Kang, S. Pei, C. Zhang, G. Zhang, Y. Zhou, L. Fan, Q. Yao, W. Wang, S. Shuang and C. Dong, A red emitting fluorescent probe based on TICT for selective detection and imaging of HSA, *Spectrochim. Acta, Part A*, 2021, **250**, 119409.
145 S. Pei, J. Li, N. Kang, G. Zhang, B. Zhang, C. Zhang and S. Shuang, Synthesis of a new environment-sensitive fluorescent probe based on TICT and application for detection of human serum albumin and specific lipid droplets imaging, *Anal. Chim. Acta*, 2022, **1190**, 339267.
146 S. Pei, J. Li, C. Zhang, G. Zhang, Y. Zhou, L. Fan, W. Wang, S. Shuang and C. Dong, TICT-Based Microenvironment-Sensitive Probe with Turn-on Red Emission for Human Serum Albumin Detection and for Targeting Lipid Droplet Imaging, *ACS Biomater. Sci. Eng.*, 2022, **8**, 253–260.
147 Y.-D. Deng, Q. Liu, D. Wang, Z.-W. Pan, T.-T. Du, Z.-X. Yuan and W.-J. Yi, Bridged triphenylamine-based fluorescent probe for selective and direct detection of HSA in urine, *Bioorg. Chem.*, 2024, **152**, 107742.
148 Z. Chen, Z. Xu, T. Qin, D. Wang, S. Zhang, T. Lv, L. Wang, X. Chen, B. Liu and X. Peng, Rational design of donor-acceptor fluorescent probe for the ratiometric point-of-care testing of human serum albumin, *Sens. Actuators, B*, 2024, **398**, 134687.
149 Y. Huyan, X. Nan, H. Li, S. Sun and Y. Xu, A novel FA1-targeting fluorescent probe for specific discrimination and identification of human serum albumin from bovine serum albumin, *Chem. Commun.*, 2024, **60**, 3810–3813.
150 S. Casey Laizure, V. Herring, Z. Hu, K. Witbrodt and R. B. Parker, The Role of Human Carboxylesterases in Drug Metabolism: Have We Overlooked Their Importance?, *Pharmacotherapy*, 2013, **33**, 210–222.
151 T. Satoh and M. Hosokawa, THE MAMMALIAN CARBOXYLESTERASES: From Molecules to Functions, *Annu. Rev. Pharmacol. Toxicol.*, 1998, **38**, 257–288.
152 D. Wang, L. Zou, Q. Jin, J. Hou, G. Ge and L. Yang, Human carboxylesterases: a comprehensive review, *Acta Pharm. Sin. B*, 2018, **8**, 699–712.
153 K. Na, E.-Y. Lee, H.-J. Lee, K.-Y. Kim, H. Lee, S.-K. Jeong, A.-S. Jeong, S. Y. Cho, S. A. Kim, S. Y. Song, K. S. Kim, S. W. Cho, H. Kim and Y.-K. Paik, Human plasma carboxylesterase 1, a novel serologic biomarker candidate for hepatocellular carcinoma, *Proteomics*, 2009, **9**, 3989–3999.
154 X. Rong, X. Li, C. Liu, C. Wu, Z. Wang and B. Zhu, Dual-reporter fluorescent probe for precise identification of liver cancer by sequentially responding to carboxylesterase and polarity, *Talanta*, 2024, **278**, 126477.
155 Y.-L. Qi, H.-R. Wang, L.-L. Chen, B. Yang, Y.-S. Yang, Z.-X. He and H.-L. Zhu, Multifunctional Fluorescent Probe for Simultaneously Detecting Microviscosity, Micropolarity, and Carboxylesterases and Its Application in Bioimaging, *Anal. Chem.*, 2022, **94**, 4594–4601.
156 S. Zhang, H. Chen, L. Wang, X. Qin, B.-P. Jiang, S.-C. Ji, X.-C. Shen and H. Liang, A General Approach to Design Dual Ratiometric Fluorescent and Photoacoustic Probes for Quantitatively Visualizing Tumor Hypoxia Levels In Vivo, *Angew. Chem., Int. Ed.*, 2022, **61**, e202107076.
157 K. M. Atkinson, J. J. Morsby, S. S. R. Kommidi and B. D. Smith, Generalizable synthesis of bioresponsive near-infrared fluorescent probes: sulfonated hepta-

methine cyanine prototype for imaging cell hypoxia, *Org. Biomol. Chem.*, 2021, **19**, 4100–4106.
158 Y.-L. Qi, H.-R. Wang, Q.-J. Kang, L.-L. Chen, P.-F. Qi, Z.-X. He, Y.-S. Yang and H.-L. Zhu, A versatile fluorescent probe for simultaneously detecting viscosity, polarity and nitroreductases and its application in bioimaging, *Sens. Actuators, B*, 2022, **352**, 130989.
159 B. Levine and G. Kroemer, Autophagy in the Pathogenesis of Disease, *Cell*, 2008, **132**, 27–42.
160 B. Levine and G. Kroemer, Biological Functions of Autophagy Genes: A Disease Perspective, *Cell*, 2019, **176**, 11–42.
161 G. Mariño, M. Niso-Santano, E. H. Baehrecke and G. Kroemer, Self-consumption: the interplay of autophagy and apoptosis, *Nat. Rev. Mol. Cell Biol.*, 2014, **15**, 81–94.
162 N. T. Ktistakis and S. A. Tooze, Digesting the Expanding Mechanisms of Autophagy, *Trends Cell Biol.*, 2016, **26**, 624–635.
163 M. Mandic, V. Paunovic, L. Vucicevic, M. Kosic, S. Mijatovic, V. Trajkovic and L. Harhaji-Trajkovic, No energy, no autophagy-Mechanisms and therapeutic implications of autophagic response energy requirements, *J. Cell. Physiol.*, 2024, **239**, e31366.
164 W.-L. Jiang, Z.-Q. Wang, Z.-K. Tan, G.-J. Mao, J. Fei and C.-Y. Li, A dual-response fluorescent probe for simultaneously monitoring polarity and ATP during autophagy, *J. Mater. Chem. B*, 2022, **10**, 4285–4292.
165 T. Zhu, Y. Hu, X. Chen, H. Shao, Z. Chen, H. Zhang and C. Liu, Novel chromene-derived fluorescent probe for detection of cyanides by imine-controlled ESIPT, *Dyes Pigm.*, 2021, **195**, 109693.
166 T. Peng, J. Chen, R. Liu and J. Qu, A benzothiophene-based fluorescent probe with dual-functional to polarity and cyanide for practical applications in living cells and real water samples, *Spectrochim. Acta, Part A*, 2024, **314**, 124198.
167 C. Kondo, K. Shibata, M. Terauchi, H. Kajiyama, K. Ino, S. Nomura, A. Nawa, S. Mizutani and F. Kikkawa, A novel role for placental leucine aminopeptidase (P-LAP) as a determinant of chemoresistance in endometrial carcinoma cells, *Int. J. Cancer*, 2006, **118**, 1390–1394.
168 M. Matsui, J. H. Fowler and L. L. Walling, Leucine aminopeptidases: diversity in structure and function, *Biol. Chem.*, 2006, **387**, 1535–1544.
169 K. Shibata, K. Shibata, F. Kikkawa, F. Kikkawa, Y. Mizokami, Y. Mizokami, H. Kajiyama, H. Kajiyama, K. Ino, K. Ino, S. Nomura, S. Nomura, S. Mizutani and S. Mizutani, Possible Involvement of Adipocyte-Derived Leucine Aminopeptidase via Angiotensin II in Endometrial Carcinoma, *Tumour Biol.*, 2005, **26**, 9–16.
170 Y. Chen, Fluorescent probes for detection and bioimaging of leucine aminopeptidase, *Mater. Today Chem.*, 2020, **15**, 100216.
171 R. Li, J. Guo, Y. Duan, X. Liu, L. Gui, Y. Xu, X. Kong, Y. Li, H. Chen and Z. Yuan, Monitoring inflammation-cancer progression by cell viscosity, polarity and leucine aminopeptidase using multicolor fluorescent probe, *Chem. Eng. J.*, 2022, **435**, 135043.
172 N. Ahmed, W. Zareen, D. Zhang, X. Yang and Y. Ye, Coumarin-Based Reversible Fluorescent Probe for Selective Detection of $Cu2^{+}$ in Living Cells, *J. Fluoresc.*, 2020, **30**, 1171–1179.
173 Y. Chen, S. Zheng, M. H. Kim, X. Chen and J. Yoon, Recent progress of TP/NIR fluorescent probes for metal ions, *Curr. Opin. Chem. Biol.*, 2023, **75**, 102321.
174 D. Li, L. Gong, Z. Qiao, C. Zhu, Q. Jia, H. Kong and S. Jiao, A highly selective colorimetric fluorescence probe for Cu^{2+} in aqueous media: the synthesis, DFT investigation and its application in living cells, *Anal. Methods*, 2020, **12**, 943–950.
175 L. Deng, Y. Cheng, L. Xue, Y. Gao, S. Fu and H. Wang, A novel coumarin based fluorescent sensor for high-sensitive detection of Cu^{2+} and water as well as applications in food and environmental analysis, *Dyes Pigm.*, 2024, **231**, 112399.
176 W. Wan, L. Zeng, W. Jin, X. Chen, D. Shen, Y. Huang, M. Wang, Y. Bai, H. Lyu, X. Dong, Z. Gao, L. Wang, X. Liu and Y. Liu, A Solvatochromic Fluorescent Probe Reveals Polarity Heterogeneity upon Protein Aggregation in Cells, *Angew. Chem., Int. Ed.*, 2021, **60**, 25865–25871.

